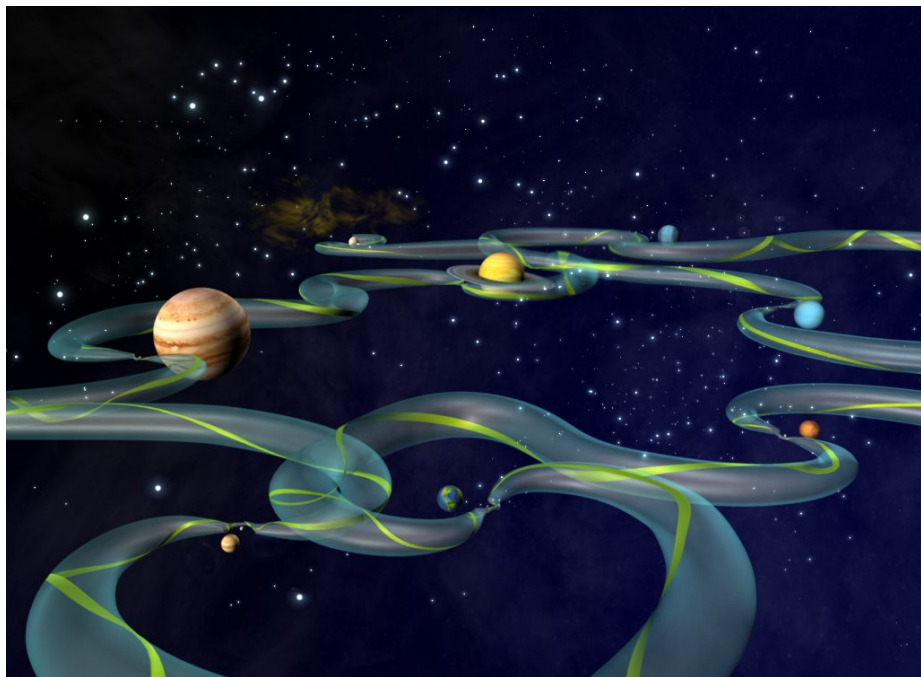


Interplanetary Trajectory Design using Dynamical Systems Theory

THESIS REPORT

by Linda van der Ham



8 February 2012

The image on the front is an artist impression of the Interplanetary Superhighway [NASA, 2002].

Preface

This MSc. thesis forms the last part of the curriculum of Aerospace Engineering at Delft University of Technology in the Netherlands. It covers subjects from the MSc. track Space Exploration, focusing on astrodynamics and space missions, as well as new theory as studied in the literature study performed previously.

Dynamical Systems Theory was one of those new subjects, I had never heard of before. The existence of a so-called Interplanetary Transport Network intrigued me and its use for space exploration would mean a total new way of transfer. During the literature study I did not find any practical application of the theory to interplanetary flight, while it was stated as a possibility. This made me wonder whether it was even an option, a question that could not be answered until the end of my thesis work.

I would like to thank my supervisor Ron Noomen, for his help and enthusiasm during this period; prof. Wakker for his inspirational lectures about the wonders of astrodynamics; the Tudat group, making research easier for a lot of students in the future.

My parents for their unlimited support in every way. And Wouter, for being there.

Thank you all and enjoy!

Abstract

In this thesis, manifolds in the coupled planar circular restricted three-body problem (CR3BP) as means of interplanetary transfer are examined. The equations of motion or differential equations of the CR3BP are studied according to Dynamical Systems Theory (DST).

This study yields the well-known Lagrange equilibrium points or libration points. The theory can be developed further to also yield periodic orbits around these points. From these periodic orbits, asymptotic paths or manifolds are generated, which leave or approach them. Plotting the manifolds for two neighboring Sun-planet systems, according to the planet positions, shows new possibilities for interplanetary transfer. Finally the optimal high-thrust maneuver in place and time to connect trajectories on overlapping manifolds is found. This minimal velocity increment ΔV is used in the design of a mission, to analyze its feasibility.

The implemented techniques to compute libration points, periodic orbits, energy levels and manifolds give accurate results. Based on the analysis of energy levels and overlap in manifolds for minimum energy levels, the connection between the Sun-Jupiter and Sun-Saturn system is used for optimization. Over a synodic period of 20 years, the minima show cyclic behaviour. The best time and place of connection is mostly dependent on orientation of the manifolds with respect to each other and could therefore already be derived from the plots of overlapping manifolds. Optimization through a grid search yields a ΔV of 200 m/s, which makes manifolds a promising way of transfer from one system to another.

For the total transfer from a parking orbit about Jupiter to a parking orbit about Saturn, however, the examined transfer using manifolds is not to be preferred over a classical Hohmann orbit. Both the ΔV budget and the transfer time are higher. The manifolds should therefore be used in another type of mission, especially to and between the outer planets and their libration points.

Contents

Preface	i
Abstract	iii
Symbols	vii
Abbreviations	ix
1 Introduction	1
1.1 Study	1
1.2 Report	2
2 Astrodynamics	5
2.1 Motion of a body	5
2.2 Two-body problem	6
2.3 Gravity assists	7
2.4 Circular restricted three-body problem	9
2.5 Energy in a system of three bodies	11
2.6 Lagrange Libration points	12
3 Libration points	15
3.1 Determination of libration points	15
3.2 Results and verification	15
4 Dynamical Systems Theory	17
4.1 Introduction	17
4.2 Motion in the PCR3BP	19
4.3 Extension to the spatial case and 4-body problem	21
5 Periodic orbits	25
5.1 Differential correction	25
5.2 Results and verification	26
6 Manifolds	33
6.1 Generation of manifolds	33
6.2 Results from Tudat	33
6.3 Verification and comparison	35
7 Coupling two planar CR3BP's	37
7.1 Coupled 3-body systems	37
7.2 Analysis of energy levels	39
7.3 Possibilities for transfer	41
8 Intersections in the coupled PCR3BP	47
8.1 Poincaré sections	47
8.2 Other cuts	48
8.3 Other epochs	49
8.4 Analysis	53

9 Discussion of results	59
9.1 Comparison to Hohmann transfer	59
9.2 Feasibility of the mission	61
10 Conclusions and Recommendations	63
References	67
Appendix A: Numerical integration	71
RK integrators	71
Variable step size	72
Appendix B: Tudat	73
Development	73
Additions	73
Appendix C: AUTO	75
Theory	75
Usage	76

Symbols

Symbol	Description	Units
α	asymptotic deflection angle	
β	incoming swing-by angle	
Δ	increment	
δ	partial differential	
Φ	increment function	
Φ	state transition matrix	
γ	imaginary eigenvalue	
η	component rotating reference frame	
λ	eigenvalue	
λ	Floquet multiplier	
μ	gravitational parameter	km^3s^{-2}
μ	dimensionless mass parameter	
μ	parameters	
Σ	cross-section	
θ	true anomaly	
θ	angular position	
τ	real eigenvalue	
v	real eigenvalue	
ω	angular velocity	s^{-1}
ξ	component rotating reference frame	
ζ	component rotating reference frame	

Latin symbols can be found on the next page.

Symbol	Description	Units
A	coefficient	
A	amplitude	
A	constant matrix	
a	semi-major axis	m
a	RK coefficient	
B	coefficient	
b	semi-minor axis	m
b	RK coefficient	
C	Jacobian energy constant	$m^2 s^{-2}$
c	constant	
c	RK coefficient	
d	differential	
d	distance	
d	deviation	
E	energy	$m^2 s^{-2}$
e	eccentricity	
e	error	
\bar{e}	unit vector	
F	matrix linearized equations of motion	
f	function	
G	gravitational constant	$m^3 kg^{-1} s^{-2}$
h	step size	
I	identity matrix	
i	index	
j	index	
K	second order derivative function	
k	RK derivative function	
M	mass	kg
m	mass	kg
n	dimension	
O	origin	
P	points	
P	Poincaré-map	
p	semi-latus rectum	m
r	radius	m
r	position	m
s	RK index	
t	time	s
T	period	s
U	potential	$m^2 s^{-2}$
u	eigenvector	
V	scalar velocity	ms^{-1}
V	collection	
v	velocity vector	ms^{-1}
v	eigenvector	
W_s	stable manifold	
W_u	unstable manifold	
w	eigenvector	
x	position component	m
x	position vector	m
y	position component	m
z	position component	m

Abbreviations

AU	Astronomical Unit
BVP	Boundary Value Problem
CR3BP	Circular Restricted Three-Body Problem
CR4BP	Circular Restricted Four-Body Problem
DST	Dynamical Systems Theory
E	Exterior region
J2000	Julian standard epoch 2000
I	Interior region
in	inertial
L	Libration point
NASA	National Aeronautics and Space Administration
NI	No Intersection
PCR3BP	Planar CR3BP
R	Equilibrium region
RK	Runge-Kutta
RKF	Runge-Kutta-Fehlberg
SI	Standard International units
std	standard deviation
STM	State Transition Matrix
TBD	To Be Determined
Tudat	Technical University Delft Astrodynamics Toolbox
wrt	with respect to

1 Introduction

Due to the gravitational attraction of the many bodies in our solar system, comets (for example) do not precisely fly the conic sections we nowadays use for spaceflight. Not having any means of propulsion, they naturally follow the most energy-efficient orbits for transfer. As energy is one of the major constraints in the design of a space mission, making use of the paths that these subtle gravitational effects create could therefore particularly offer a great advantage for interplanetary space flight.

1.1 Study

The subject of this thesis is the use of manifolds, as these paths are called, for interplanetary transfer. Instead of the two-body problem commonly used in mission design, three bodies are considered simultaneously: the satellite, a planet and the Sun. Knowing that planet and Sun orbit one another in almost circular orbits, and the mass of the satellite is negligible compared to the mass of these bodies, the model of the circular restricted three-body problem (CR3BP) can be used [Wakker, 2007a].

Dynamical Systems Theory (DST) concerns itself with the analysis of differential equations, as the equations of motion in the CR3BP are. After finding equilibrium points (both velocity and acceleration are zero), the region about this points can be examined. Periodic orbits and asymptotic orbits are two of the four types of motion in these regions [Conley, 1968]. The asymptotic paths are also called manifolds, which form a natural highway to travel from and to the area around equilibrium points, as is shown in Figure 1. Extending the manifolds far from the periodic orbits for many Sun-planet systems shows a network of manifold tubes, which is referred to as the Interplanetary Superhighway [NASA, 2002].

Zooming in on two consecutive Sun-planet systems the transfer from one to another can be examined. The actual four-body problem is approximated by two coplanar coupled three-body problems [Koon, 2006].

In this study the high-trust maneuver requiring the minimal instantaneous velocity increment to get from one CR3BP to the next, is to be found. On the intersection of manifolds, different positions for executing the maneuver are available. Furthermore the mutual geometry of the two systems changes with the chosen epoch. So for changing place and time of the maneuver, the minimal velocity increment is computed and analyzed. Finally the optimal maneuver is used in the design of a mission; a transfer from one planet to another. Addressing the feasibility of such a mission is the final goal of this study.

Computations are mainly performed using the Technical University Delft Astrodynamics Toolbox (Tudat), a C++ library for astrodynamics simulations [Tudat, 2011]. New functions needed during the study have been implemented according to the theory in this report and added to the toolbox. The report therefore also contains verification of these computations.

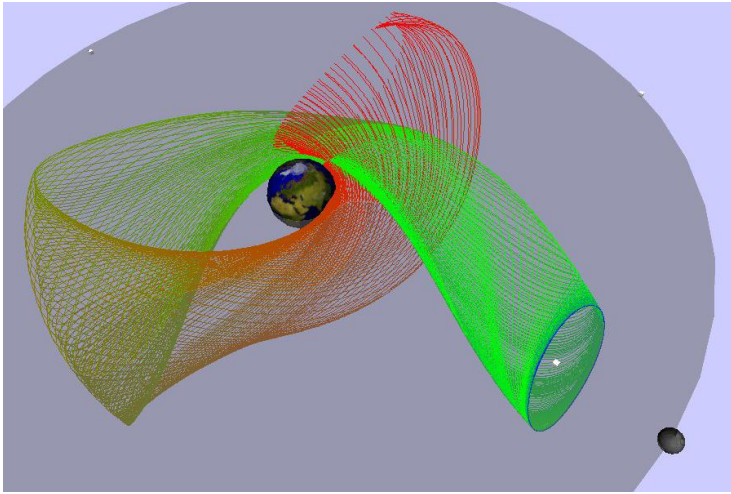


Figure 1: A manifold extending from a periodic orbit about an equilibrium point in the Earth-Moon three-body system [Doedel, 2010].

1.2 Report

To understand the subject and answer this study's main questions, first basic theory of astrodynamics and DST is presented. Starting from the many-body problem, the equations of motion of the CR3BP are derived in Chapter 2. Analysis of these equations and the Jacobi energy integral shows the existence of libration points. The chapter also covers the two-body problem, which is used later for comparison.

In Chapter 3 the positions of libration points are calculated and checked against values from literature and AUTO, a tool to analyze ordinary differential equations.

After some important concepts from DST are introduced in Chapter 4, the theory is applied to the planar CR3BP (PCR3BP). Linearizing the equations of motion different types of motion in the near-equilibrium area about libration points can be identified, such as periodic orbits and asymptotic orbits, also known as manifolds. It will be shown how the theory can be extended to the spatial case and a system of four bodies.

Chapter 5 explains how the periodic orbits can be found by differential correction. The sensitivity of the technique to changes in initial position and energy level are discussed and the resulting periodic orbits are verified.

Next the generation of manifolds is presented in Chapter 6. A method for the optimal choice of the size of deviation from the periodic orbit is shown and results are tested. From each periodic orbit now a family of orbits, forming a manifold, can be generated.

The results of the PCR3BP are typically expressed in normalized parameters (position, velocity, time). However, for the coupling of two three-body systems, these quantities have to be converted to standard units and an inertial reference frame. Chapter 7 shows how to do this and analyses minimum and maximum energy levels. Coupling the systems of any pair of neighboring planets and their manifolds then shows the possibilities for interplanetary transfer.

For the most suitable coupled three-body systems, the maneuver to change from one three-body system to the next is computed in Chapter 8. The minimal velocity increment for different places on intersecting manifolds and at different epochs is calculated and the behaviour of these minima is analyzed.

In Chapter 9 this minimal velocity increment is used in the design of an interplanetary mission. It is compared to a classical Hohmann transfer and its feasibility is discussed.

This all leads to the conclusions and recommendations in the final chapter.

2 Astrodynamics

In this chapter the basic theory of astrodynamics needed to understand DST is presented. It focuses on an analysis of the CR3BP and the equilibrium points in this system. All theory is based on the lecture notes Astrodynamics I [Wakker, 2007a].

2.1 Motion of a body

Defining all planets, moons and satellites, as point masses, they all have an attracting influence on each other. Under the assumption that no forces other than gravity are present, the motion of one body (i) with respect to an inertial reference frame is driven by the gravitational attraction of all other bodies in the system, and can be written as:

$$m_i \frac{d^2 \bar{r}_i}{dt^2} = \sum_j^* G \frac{m_i m_j}{r_{ij}^3} \bar{r}_{ij} \quad (1)$$

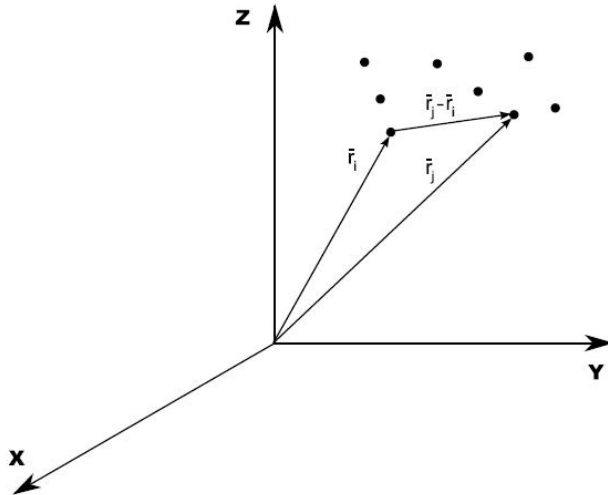


Figure 2: A system of bodies with respect to an inertial reference frame [Kumar, 2008].

Here m is mass, G is the universal constant of gravitation and $*$ indicates all bodies j excluding $j = i$. The position vector \bar{r}_{ij} describes the position of the body j relative to body i , as shown in Figure 2. When only focusing on two bodies and regarding the influence of the others as disturbing accelerations (initially neglected), analytical solutions are available. They result in for example the equations for Keplerian motion, as shown in Section 2.2. However, when taking three bodies into account, no general(!) analytic solutions are available. The motion of one of the three bodies $\{1, 2, 3\}$ is defined by:

$$\frac{d^2 \bar{r}_1}{dt^2} = G \frac{m_2}{r_{12}^3} \bar{r}_{12} + G \frac{m_3}{r_{13}^3} \bar{r}_{13} \quad (2)$$

Expressing the vectors relatively ($\bar{r}_{12} = \bar{r}_2 - \bar{r}_1$ and $\frac{d^2\bar{r}_{12}}{dt^2} = \frac{d^2\bar{r}_2}{dt^2} - \frac{d^2\bar{r}_1}{dt^2}$) results in the Lagrange formulation (Figure 3):

$$\frac{d^2\bar{r}_{12}}{dt^2} = G \left[m_3 \left(\frac{\bar{r}_{23}}{r_{23}^3} + \frac{\bar{r}_{31}}{r_{31}^3} \right) - (m_1 + m_2) \frac{\bar{r}_{12}}{r_{12}^3} \right] \quad (3)$$

The equation exists respectively of a term accounting for the effective attraction by the third body and a strictly 2-body term. The latter one can be solved analytically.

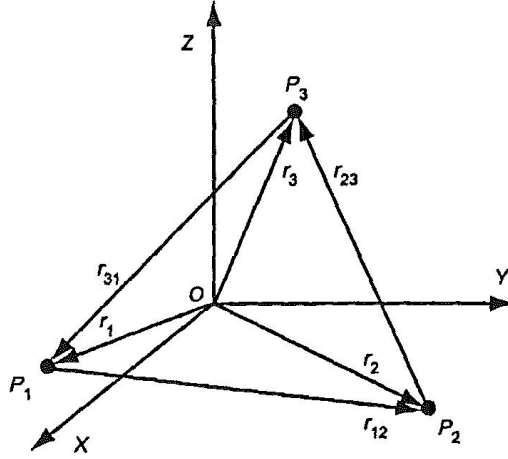


Figure 3: Geometry of the system of three bodies and vectors used in classical and Lagrange formulation [Wakker, 2007a].

2.2 Two-body problem

With the Lagrange formulation of Equation 3, the equation of motion of the two-body problem can be written as:

$$\frac{d^2\bar{r}_{12}}{dt^2} = -G(m_1 + m_2) \frac{\bar{r}_{12}}{r_{12}^3} \quad (4)$$

With $\mu = G(m_1 + m_2) \approx Gm_1$, the relative motion of a body 2 about a much larger body 1 becomes:

$$\ddot{\bar{r}} = -\mu \frac{\bar{r}}{r^3} \quad (5)$$

The solution of this equation of motion is referred to as *Keplerian motion* and describes a conic section with the massive body in the focal point:

$$r = \frac{p}{1 + e \cos(\theta)} \quad (6)$$

For an elliptical orbit as shown in Figure 4 the closest point ($\theta = 0$, A) is called the pericenter and the furthest point is called the apocenter ($\theta = \pi$, A'). Substituting their positions in Equation 6 yields:

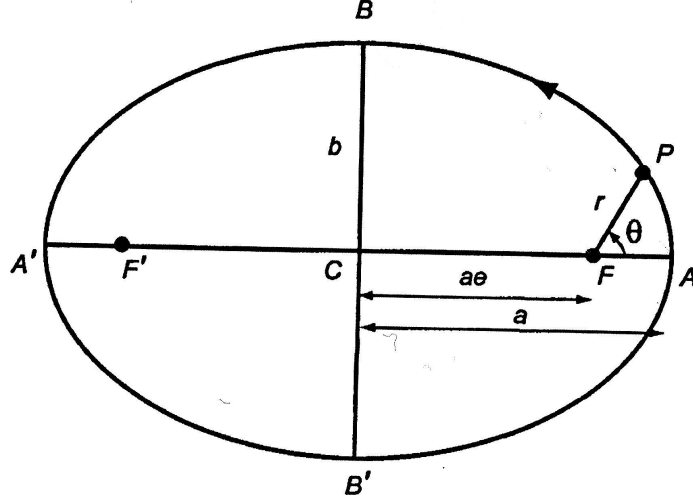


Figure 4: Geometry of an elliptical orbit [Wakker, 2007a].

$$p = a(1 - e^2) \quad (7)$$

Taking the scalar product of Equation 5 and $\dot{\vec{r}}$ and integration yields:

$$\frac{1}{2}V^2 - \frac{\mu}{r} = \text{constant} \quad (8)$$

With this equation the velocity V at any point along a Keplerian orbit can be computed.

When using instantaneous velocity increments (ΔV) the Keplerian transfer to a higher orbit requiring the least amount of them turns out to be a Hohmann orbit. It has its pericenter on the original orbit of the satellite and its apocenter on the target orbit, which are all assumed to be circular and coplanar. The time needed for this transfer is half of the orbital period of an ellipse, which is known because of Kepler's third law:

$$T_{\text{Hohmann}} = \frac{1}{2}T_{\text{ellipse}} = \pi \sqrt{\frac{a^3}{\mu}} \quad (9)$$

By regarding the multiple body system as a succession of patches in which the satellite is only attracted by one dominating body (so a series of two-body problems), a large number of missions have been designed. The total ΔV and transfer time coming out of such a model typically serve as a reference in comparison with the values of non-Keplerian orbits, such as the ones discussed in this report.

2.3 Gravity assists

Another possibility in the two-body problem is hyperbolic motion, for which the eccentricity $e > 1$ and the planet is again in the focal point. The energy or velocity of the satellite is too high to stay in an elliptical orbit about the planet.

The change in velocity of the spacecraft according to Figure 5 is [Wakker, 2007b]:

$$\Delta V = 2V_\infty \sin \frac{1}{2}\alpha \quad (10)$$

At a swing-by distance r_3 , the asymptotic deflection angle is defined by:

$$\sin \frac{1}{2}\alpha = \frac{1}{1 + r_3 V_\infty^2 \mu^{-1}} \quad (11)$$

With the definition of energy as the sum of kinetic and potential energy, and the change in potential energy being negligible, this leads to a difference in inertial energy of:

$$\Delta E = \frac{1}{2}(V_4^2 - V_2^2) = 2V_t V_\infty \sin \frac{1}{2}\alpha \cos \beta \quad (12)$$

Here the swing-by angle β is determined by the satellite's incoming trajectory with respect to the planet. Notice that the inertial energy E will decrease when passing before the planet ($90^\circ < \beta < 270^\circ$) and increase when passing behind the planet.

The maximum difference is achieved for r_3 being minimal, or a swing-by as close to the surface of the planet as possible. The maximal increase in energy is found for $\beta = 0^\circ$.

2.4 Circular restricted three-body problem

As said before, for systems consisting of more than 2 bodies no general analytical solutions are possible. However, in practical cases some assumptions for multi-body systems can be made. For the Circular Restricted Three-Body Problem (CR3BP), they are:

- The mass of two bodies is much larger than the mass of the third body. Therefore the effect of the gravitational attraction of the third body on the motion of the other two can be neglected.
- The two massive bodies move in circular orbits about the centre of mass of the system and thus also about each other.

This is a valid assumption when for example the third body is a spacecraft and the other two bodies are two planets or a planet and a moon, in orbits with low eccentricities.

The plane in which the two massive bodies now move about each other defines the reference frame X, Y, Z , which rotates with respect to the inertial reference frame ξ, η, ζ . In this rotating reference frame the X -axis is in the direction of \bar{r}_{12} and the ζ and Z axes coincide. So the reference frame rotates about the ζ -axis with a constant angular velocity ω . In Figure 6 and in coming equations the index 3 is dropped, such that $\bar{r}_3 = \bar{r}$, $\bar{r}_{13} = \bar{r}_1$ and $\bar{r}_{23} = \bar{r}_2$.

The motion of the third body, described by Equation 2, is not restricted to this plane and is defined with respect to the inertial reference frame by:

$$\frac{d^2 \bar{r}}{dt^2} = -G \frac{m_1}{r_1^3} \bar{r}_1 - G \frac{m_2}{r_2^3} \bar{r}_2 \quad (13)$$

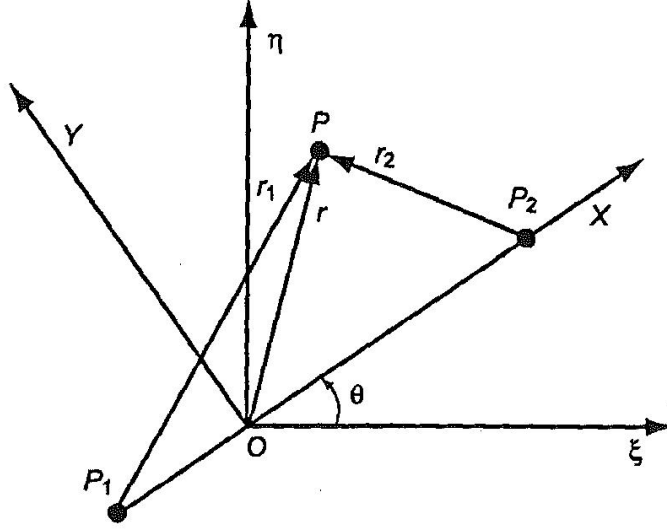


Figure 6: Inertial and rotating reference frames in the CR3BP [Wakker, 2007a].

The velocity of the third body with respect to the inertial reference frame is defined as $\frac{d\bar{r}}{dt}$ and with respect to the rotating (with angular velocity ω) reference frame as $\frac{\delta\bar{r}}{\delta t}$, such that:

$$\frac{d\bar{r}}{dt} = \frac{\delta\bar{r}}{\delta t} + \bar{\omega} \times \bar{r} \quad (14)$$

Differentiation and substitution in Equation 13 gives the motion of the third body with respect to the rotating reference frame:

$$\frac{\delta^2\bar{r}}{\delta t^2} = -G \left(\frac{m_1}{r_1^3} \bar{r}_1 + \frac{m_2}{r_2^3} \bar{r}_2 \right) - 2\bar{\omega} \times \frac{\delta\bar{r}}{\delta t} - \bar{\omega} \times (\bar{\omega} \times \bar{r}) \quad (15)$$

Normalizing mass (to $m_1 + m_2$), distance (to r_{12}) and time (to $\frac{1}{\omega}$), the problem is only depending on the mass parameter $\mu = \frac{m_2}{m_1 + m_2}$:

$$\frac{\delta^2\bar{r}}{\delta t^2} = - \left(\frac{1-\mu}{r_1^3} \bar{r}_1 + \frac{\mu}{r_2^3} \bar{r}_2 \right) - 2\bar{e}_z \times \frac{\delta\bar{r}}{\delta t} - \bar{e}_z \times (\bar{e}_z \times \bar{r}) \quad (16)$$

With the new units the previously defined position vectors relative to the rotating reference frame become:

$$\begin{aligned} \bar{r} &= x\bar{e}_x + y\bar{e}_y + z\bar{e}_z \bar{r}_1 = (\mu + x)\bar{e}_x + y\bar{e}_y + z\bar{e}_z \\ \bar{r}_2 &= -(1 - \mu - x)\bar{e}_x + y\bar{e}_y + z\bar{e}_z \end{aligned} \quad (17)$$

Now Equation 16 can be split into three scalar equations:

$$\begin{aligned} \ddot{x} &= - \left(\frac{1-\mu}{r_1^3} \right) (\mu + x) + \frac{\mu}{r_2^3} (1 - \mu - x) + 2\dot{y} + x \\ \ddot{y} &= - \left(\frac{1-\mu}{r_1^3} \right) y - \frac{\mu}{r_2^3} y - 2\dot{x} + y \\ \ddot{z} &= - \left(\frac{1-\mu}{r_1^3} \right) z - \frac{\mu}{r_2^3} z \end{aligned} \quad (18)$$

When a scalar function $U = \frac{1}{2}(x^2 + y^2) + \frac{1-\mu}{r_1} + \frac{\mu}{r_2}$ is defined, it turns out to serve as a potential function:

$$\begin{aligned}\ddot{x} - 2\dot{y} &= \frac{\delta U}{\delta x} \\ \dot{y} + 2\dot{x} &= \frac{\delta U}{\delta y} \\ \ddot{z} &= \frac{\delta U}{\delta z}\end{aligned}\tag{19}$$

The potential U is conservative and non-central. After manipulation it can be used to construct an integral of motion for the three-body problem, as shown in the next section.

There are also other ways to find these equations of motion, such as Hamiltonian mechanics. The theory as presented here is preferred because of its simplicity and obvious physical interpretation.

2.5 Energy in a system of three bodies

Multiplication of Equations 19 with respectively \dot{x} , \dot{y} and \dot{z} and summation yields:

$$\dot{x}\ddot{x} + \dot{y}\ddot{y} + \dot{z}\ddot{z} = \dot{x}\frac{\delta U}{\delta x} + \dot{y}\frac{\delta U}{\delta y} + \dot{z}\frac{\delta U}{\delta z} = \frac{dU}{dt}\tag{20}$$

Integration of all terms results in Jacobi's integral:

$$\dot{x}^2 + \dot{y}^2 + \dot{z}^2 = 2U - C\tag{21}$$

Or, with V being the velocity of the third body with respect to the rotating reference frame:

$$V^2 = 2U - C\tag{22}$$

After substitution of the definition of U , it can also be written as:

$$C = x^2 + y^2 + \frac{2(1-\mu)}{r_1} + \frac{2\mu}{r_2} - V^2\tag{23}$$

When the velocity of the third body V is zero, this equation describes the surfaces of Hill. For any real body $V^2 \geq 0$, such that these surfaces describe which regions of the XYZ-space are accessible for the third body:

$$2U = x^2 + y^2 + \frac{2(1-\mu)}{r_1} + \frac{2\mu}{r_2} \geq C\tag{24}$$

For example in the XY-plane ($z = 0$) the surfaces for decreasing values of the energy C and a given μ look like the curves in Figure 7. Because $2U = C$ on these curves, for all shown curves U is a constant.

In general, the accessible inner area is called the *Interior* region (I) and the outer area is called the *Exterior* region (E). For some levels of energy, the accessible area about the second massive body (m_2) becomes large enough, such that a neck between these regions exists (case 3 in Figure 7). This is the range of energy levels used in the remaining part of this report. As explained in the next section, the energy levels C_i correspond to the Lagrange Libration points with the same index, such that their values can easily be calculated. For small μ the result of these calculations is shown in Figure 8.

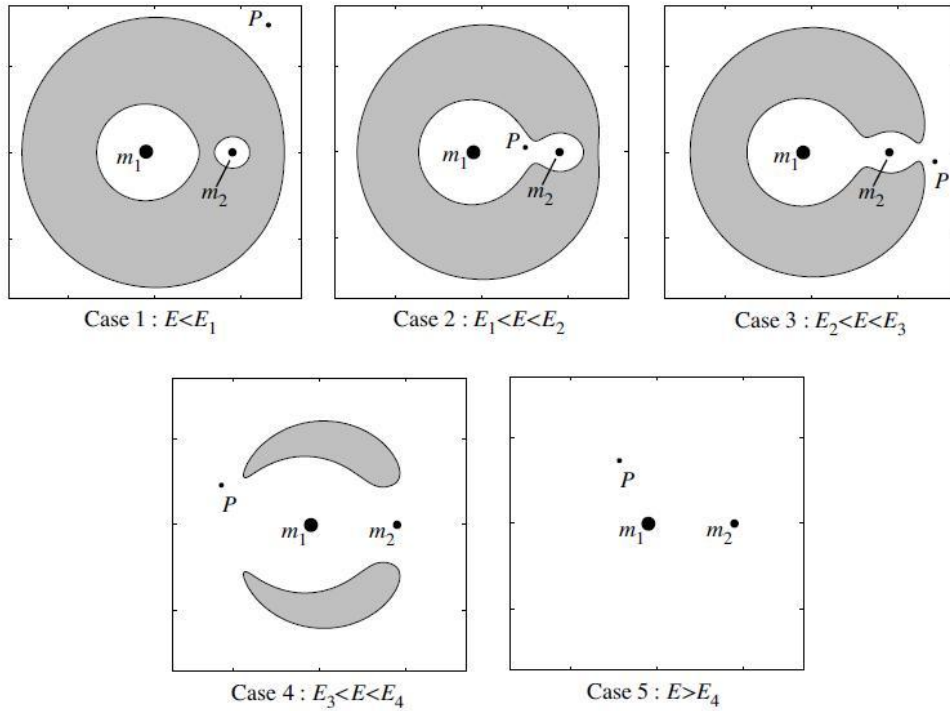


Figure 7: Hill surfaces for $z = 0$ and various levels of total energy C (denoted as $E = -\frac{1}{2}C$) [Koon, 2006].

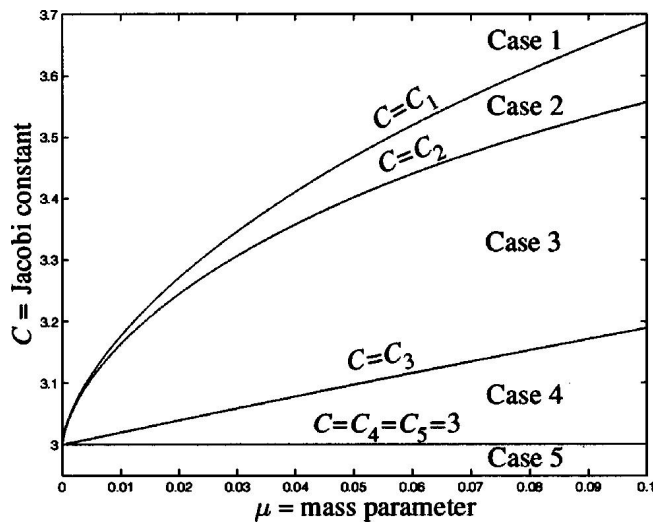


Figure 8: Energy levels C for the different cases of Figure 7 [Koon, 2000].

2.6 Lagrange Libration points

Analysis of figures like Figure 7, shows that the Hill surfaces for $z=0$ cross the X and Y axes at different places. Multiple of these crossing points may coincide

for appropriate values of C . In these coinciding points always:

$$\frac{\delta U}{\delta x} = \frac{\delta U}{\delta y} = \frac{\delta U}{\delta z} = 0 \quad (25)$$

This means that Equations 19 becomes:

$$\ddot{x} - 2\dot{y} = \ddot{y} + 2\dot{x} = \ddot{z} = 0 \quad (26)$$

Since the points are located on the surfaces where the velocity is zero:

$$\ddot{x} = \ddot{y} = \ddot{z} = 0 \quad (27)$$

In other words, also the acceleration on the third body when located in these points is zero, and the points are equilibrium points in the rotating system. They are called *Lagrange libration points* and are indicated by the symbol L . Their positions can be determined by using Equations 18:

$$0 = x - \left(\frac{1-\mu}{r_1^3} \right) (\mu + x) + \frac{\mu}{r_2^3} (1 - \mu - x) \quad (28)$$

$$0 = y \left(1 - \frac{1-\mu}{r_1^3} - \frac{\mu}{r_2^3} \right) \quad (29)$$

$$0 = z \left(\frac{1-\mu}{r_1^3} + \frac{\mu}{r_2^3} \right) \quad (30)$$

Because r_1 and r_2 are positive and $0 \leq \mu \leq \frac{1}{2}$ Equation 30 yields $z = 0$. With the definitions of r_1 and r_2 (Equation 17), a first solution becomes:

$$y = 0 \quad (31)$$

$$x - (1 - \mu) - \frac{\mu + x}{|\mu + x|^3} + \mu \frac{1 - \mu - x}{|1 - \mu - x|^3} = 0 \quad (32)$$

The last equation has three real roots, resulting in L_1 , L_2 and L_3 on the X-axis, as shown in Figure 9.

The second solution, $r_1 = r_2 = 1$, is found when the term between brackets of Equation 29 equals zero. These points L_4 and L_5 thus form an equilateral triangle with the two massive bodies, and their coordinates are:

$$\begin{aligned} x &= \frac{1}{2} - \mu \\ y &= \pm \frac{1}{2} \sqrt{3} \end{aligned} \quad (33)$$

A periodic orbit about a libration point is called a Lissajous-orbit and is used frequently for observation missions. Lyapunov orbits are entirely in the plane of the two massive bodies. Halo orbits also have an out-of-plane component and have the same frequency in both parts.

In DST, libration points and orbits about them may serve as a starting point for the design of a low energy trajectory, which is explained in Chapter 4. First, in the next chapter the locations of the libration points are determined.

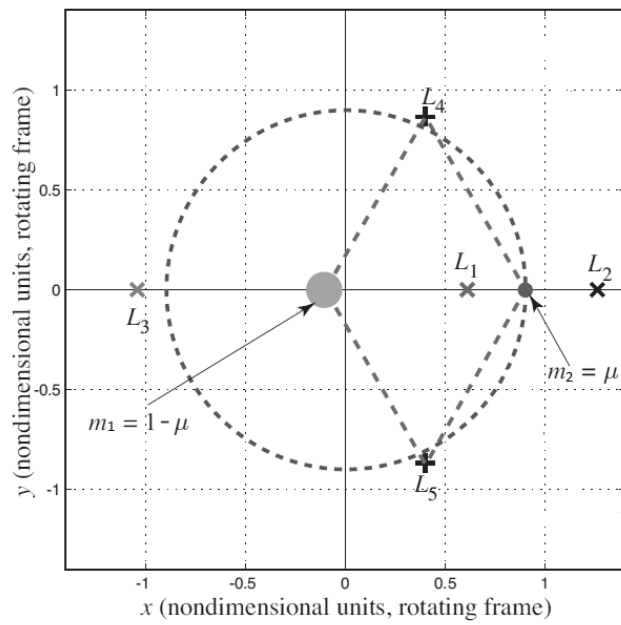


Figure 9: Position of libration points [Koon, 2006].

3 Libration points

The determination of the libration points is the first step in the design of a transfer making use of DST. It has become part of the TU Delft Astrodynamics Toolbox (Tudat), which is discussed in Appendix B. In this section its results will be verified against values from literature and results from AUTO-07p, a tool for the analysis of solutions of ordinary differential equations, discussed in Appendix C.

3.1 Determination of libration points

From Equation 18 the position in dimensionless rotating coordinates of the Lagrangian libration points can be determined. The first three points are positioned relative to the two massive bodies as shown in Figure 9. In case of L_1 this means that $-\mu < x < 1 - \mu$ or

$$\begin{aligned} |\mu + x|^3 &= (\mu + x)^3 \\ |x - (1 - \mu)|^3 &= -(x - (1 - \mu))^3 \\ -|x - (1 - \mu)|^3 &= (x - (1 - \mu))^3 \end{aligned} \quad (34)$$

The equation of motion in x-direction (32) becomes:

$$\begin{aligned} x - (1 - \mu) \frac{(\mu + x)}{|\mu + x|^3} + \mu \frac{1 - \mu - x}{|1 - \mu - x|^3} \\ = x - (1 - \mu) \frac{(\mu + x)}{(\mu + x)^3} + \mu \frac{1 - \mu - x}{(1 - \mu - x)^3} \\ = x_{L_1} - \frac{(1 - \mu)}{(\mu + x_{L_1})^2} + \frac{\mu}{(1 - \mu - x_{L_1})^2} = 0 \end{aligned} \quad (35)$$

In the same way the equations of motion for the L_2 and L_3 collinear libration points are based on their positions being limited to $-\mu < 1 - \mu < x$ and $x < -\mu < 1 - \mu$ respectively:

$$\begin{aligned} x_{L_2} - \frac{(1 - \mu)}{(\mu + x_{L_2})^2} - \frac{\mu}{(1 - \mu - x_{L_2})^2} &= 0 \\ x_{L_3} + \frac{(1 - \mu)}{(\mu + x_{L_3})^2} - \frac{\mu}{(1 - \mu - x_{L_3})^2} &= 0 \end{aligned} \quad (36)$$

Now the positions of the collinear libration points can be determined by means of a root-finding method. The positions of libration points L_4 and L_5 are computed directly via Equation 33.

3.2 Results and verification

The analytical equations and the Newton-Raphson root-finding method are used in Tudat to determine the position of the libration points for any combination of predefined celestial bodies.

For the system of Earth and Moon, the mass parameter is computed as 0.012153. This gives the location of the libration points in normalized units as shown in Table 1. Reference values are from [James, 2006] and show the correct implementation.

	Tudat		Reference values	
	x [-]	y [-]	x [-]	y [-]
L_1	0.8363	0	0.83629259089993	0
L_2	1.156	0	1.15616816590553	0
L_3	-1.005	0	-1.00511551160689	0
L_4	0.4878	0.866	0.487722529	0.86602540378444
L_5	0.4878	-0.866	0.487722529	-0.86602540378444

Table 1: Location of libration points for system of Earth and moon, via Tudat.

In the remaining part of the thesis only the L_1 and L_2 from various Sun-planet-systems are used, since these collinear libration points are situated most convenient for transfer between two neighboring planetary systems. The location of these points can also be determined via the *compute_lps* function of AUTO. Comparison of the positions (Table 2) shows no discrepancies.

	μ (Tudat)	Tudat		AUTO	
		x_{L_1} [-]	x_{L_2} [-]	x_{L_1} [-]	x_{L_2} [-]
Mercury	$1.6602 \cdot 10^{-7}$	0.996194	1.00382	9.996194	1.00388
Venus	$2.4478 \cdot 10^{-6}$	0.990682	1.00937	0.990683	1.00937
Earth	$3.0043 \cdot 10^{-6}$	0.990027	1.01003	0.990027	1.01003
Mars	$3.22712 \cdot 10^{-7}$	0.995251	1.00476	0.995254	1.00476
Jupiter	$9.53678 \cdot 10^{-4}$	0.93237	1.06883	0.93237	1.06883
Saturn	$2.85745 \cdot 10^{-4}$	0.954749	1.04607	0.954748	1.04607
Uranus	$4.3656 \cdot 10^{-5}$	0.975742	1.02457	0.975742	1.02457
Neptune	$5.14997 \cdot 10^{-5}$	0.974376	1.02596	0.974375	1.02597

Table 2: Location of libration points for system of Sun and planet, computed via Tudat and AUTO.

When dealing with smaller mass parameters, such as the ones of the Sun-Mercury, Sun-Earth and Sun-Mars systems, the AUTO precision parameters EPSL, EPSU and EPSS should be lowered. These parameters govern the relative convergence criterion [Doedel, 2009] and should also be adjusted when generating periodic orbits and manifolds using AUTO (Chapter 6).

In the next chapter, the area around libration points is analyzed by means of DST.

4 Dynamical Systems Theory

This chapter provides the theoretical background in the field of DST. It however only focuses on a general understanding of this mathematical subject. A large part of the terminology and theory is better explained in for example the book *Introduction to Applied Nonlinear Systems and Chaos* [Wiggins, 2003] which is available online. Another good source for more in-depth information is *Nonlinear Differential Equations and Dynamical Systems* [Verhulst, 2000]. After the introduction of some main concepts in DST, its application to the PCR3BP and the extension to the spatial case (CR3BP) and the 4-body problem (CR4BP) are presented.

4.1 Introduction

DST is a geometrical approach to solve differential equations. It is not only used to find low-energy trajectories for spacecraft but for example also to describe the natural motion of comets and that of atoms in molecular systems [Marsden, 2005].

The differential equation, for example shown in Equation 37, is referred to as a dynamical system. Here μ are parameters and in general the independent variable t is time. The solution or trajectory of a dynamical system can depend on initial conditions in both x and μ [Wiggins, 2003].

$$\begin{aligned}\dot{\bar{x}} &= f(x, t; \mu) \\ \bar{x} &\mapsto g(x; \mu)\end{aligned}\tag{37}$$

Poincaré mapping is a tool for the visualization of periodic orbits. The Poincaré-cut is a transversal of the orbits, forming a figure of the points where it is intersected by them. The cut is a dimension smaller than that of the orbits. It can be at any arbitrary place along an orbit, as long as it is not tangent to it and all orbits cross it in the same direction [Koon, 2006]. In Figure 10 a possible Poincaré section of a 3-dimensional problem is shown. Here V is a collection of points on the cross-section Σ , and the Poincaré-map P is the function such that $P: V \rightarrow \Sigma$.

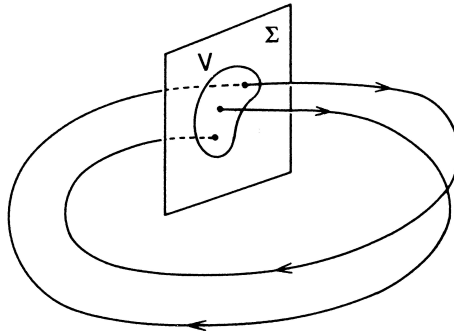


Figure 10: Geometry of the Poincaré map for a periodic orbit [Wiggins, 2003].

A manifold is defined by [Wiggins, 2003] as:

”A set which locally has the structure of Euclidean space. In applications, manifolds are most often met as m -dimensional surfaces embedded in \mathbb{R}^n . If the surface has no singular points, i.e., the derivative of the function representing the surface has maximal rank, then by the implicit function theorem it can locally be represented as a graph. The surface is a C^r manifold if the (local) graphs representing it are C^r .”

Here \mathbb{R}^n denotes the set of real numbers of dimension n ; and C^r means continuous and r times differentiable. As this definition might be hard to comprehend, in practical applications two situations can be distinguished:

- Linear: a linear vector subspace of \mathbb{R}^n .
- Nonlinear: a surface embedded in \mathbb{R}^n which can be locally represented as a graph.

An example of a manifold is a sphere, since it is the surface of a ball and can be represented by a collection of two-dimensional graphs.

An invariant manifold now is a surface defined by the property that an orbit starting on it, remains on it. So it can also be defined as a collection of orbits that together form a surface. This surface is only invariant if the vector field is always tangent to it. Manifolds approaching the invariant manifold asymptotically are called stable, the ones departing it unstable.

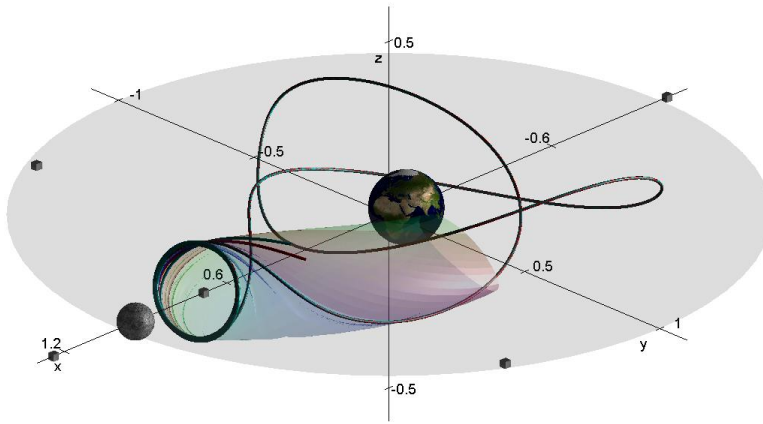


Figure 11: A homoclinic connection from a periodic (halo) orbit about L_1 [Wang, 2009].

A homoclinic trajectory is a periodic orbit that is on both the stable and unstable manifold of the same libration point, like for example the trajectory in Figure 11. When an orbit is on the stable orbit of one libration point and on the unstable one of another libration point, it is called a heteroclinic trajectory (Figure 12).

Heteroclinic connections between the L_1 libration point of a system and the L_2 of another 3-body system (or the other way around) provide means to transport the common smaller body in both systems. Because this orbit is asymptotic

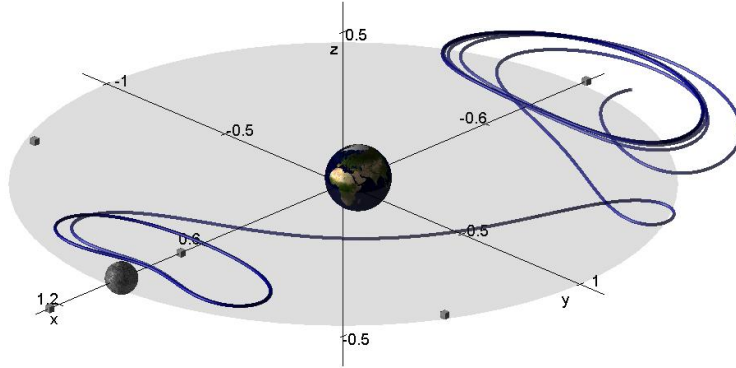


Figure 12: A heteroclinic connection between the (planar) periodic orbits about L_1 and L_3 [Wang, 2009].

no maneuvers are needed. The application to the planar, spatial and patched 3-body problems are discussed next.

4.2 Motion in the PCR3BP

In the neighborhood of a hyperbolic point (the eigenvalues of the linear vector field has non-zero real parts) the geometry of the solution of a differential equation is completely determined by the linearized system [Wiggins, 2003]. So to understand what happens in the equilibrium region (the region around the libration points, denoted as R), the equations of motion in the PCR3BP are linearized. The equations of motion (Equation 19) can be written as a system of equations:

$$\begin{aligned} \dot{x} &= \dot{x} \\ \ddot{x} &= U_x + 2\dot{y} \\ \dot{y} &= \dot{y} \\ \ddot{y} &= U_y - 2\dot{x} \end{aligned} \quad (38)$$

This system can be linearized such that it results in a matrix equation:

$$\begin{bmatrix} \dot{x} \\ \ddot{x} \\ \dot{y} \\ \ddot{y} \end{bmatrix} = \begin{bmatrix} 0 & 1 & 0 & 0 \\ U_{xx} & 0 & U_{xy} & 2 \\ 0 & 0 & 0 & 1 \\ U_{yx} & -2 & U_{yy} & 0 \end{bmatrix} \begin{bmatrix} x \\ \dot{x} \\ y \\ \dot{y} \end{bmatrix} \quad (39)$$

Here the subscripts denote the first and second partial derivatives, and $U_{xy} = U_{yx}$. By assuming $x = Ae^{\lambda t}$ and $y = Be^{\lambda t}$ the characteristic equation and the eigenvalues become:

$$\lambda^4 + \lambda^2(4 - U_{xx} - U_{yy}) + U_{xx}U_{yy} - U_{xy}^2 = 0 \quad (40)$$

$$\begin{aligned} \lambda_1 = -\lambda_2 &= \sqrt{\frac{-(4 - U_{xx} - U_{yy}) + \sqrt{(4 - U_{xx} - U_{yy})^2 - 4(U_{xx}U_{yy} - U_{xy}^2)}}{2}} \\ \lambda_3 = -\lambda_4 &= \sqrt{\frac{-(4 - U_{xx} - U_{yy}) - \sqrt{(4 - U_{xx} - U_{yy})^2 - 4(U_{xx}U_{yy} - U_{xy}^2)}}{2}} \end{aligned} \quad (41)$$

Now the linearized equations of motion become:

$$\begin{aligned} x(t) &= A_1 e^{\lambda_1 t} + A_2 e^{-\lambda_1 t} + A_3 e^{\lambda_3 t} + A_4 e^{-\lambda_3 t} \\ y(t) &= B_1 e^{\lambda_1 t} + B_2 e^{-\lambda_1 t} + B_3 e^{\lambda_3 t} + B_4 e^{-\lambda_3 t} \end{aligned} \quad (42)$$

The second-order partial derivatives for the collinear libration points (L_1 , L_2 and L_3) can be computed as:

$$\begin{aligned} K &= \frac{1-\mu}{r_1^3} + \frac{\mu}{r_2^3} \\ U_{xx} &= 1 + 2K \\ U_{xy} &= 0 \\ U_{yy} &= 1 - K \end{aligned} \quad (43)$$

Now it can be shown that the first two eigenvalues are real (exponentially in/decreasing the coordinates) and the other two are imaginary (yielding a periodic motion). In the case of the equilateral points (L_4 and L_5) and for practical values of the mass parameter ($0 < \mu < 0.0385$), the eigenvalues are all imaginary; only allowing for oscillatory motion about the libration points [Wakker, 2007a]. This is why only the collinear libration points will be used in the remaining of this study. The coefficients A_i and B_i (for $i=1..4$) are coupled via:

$$B_i = A_i \frac{\lambda_i - 2K - 1}{2\lambda_i} = A_i \gamma_i \quad (44)$$

Substituting this in Equation 42 and differentiating, shows that the eigenvectors in (x, y, \dot{x}, \dot{y}) -space are:

$$\begin{aligned} u_1 &= (1, \gamma_1, \lambda_1, \lambda_1 \gamma_1) \\ u_2 &= (1, -\gamma_1, -\lambda_1, \lambda_1 \gamma_1) \\ w_1 &= (1, \gamma_3, -\lambda_3, \lambda_3 \gamma_3) \\ w_2 &= (1, -\gamma_3, \lambda_3, \lambda_3 \gamma_3) \end{aligned} \quad (45)$$

Because both λ_3 and γ_3 are imaginary, they can be defined as $i\nu$ and $-i\tau$ respectively. And the general solution can be written as:

$$\begin{bmatrix} x(t) \\ y(t) \\ \dot{x}(t) \\ \dot{y}(t) \end{bmatrix} = A_1 e^{\lambda t} u_1 + A_2 e^{-\lambda t} u_2 + A_3 e^{i\nu t} w_1 + A_4 e^{-i\nu t} w_2 \quad (46)$$

Only the coefficients A are unknown and can be derived from the initial conditions x_0 , y_0 , \dot{x}_0 and \dot{y}_0 . Projecting the position space along the eigenvectors u_1 and u_2 of this system yields:

$$\begin{aligned} x(t) &= A_1 e^{\lambda t} + A_2 e^{-\lambda t} + A_3 e^{i\nu t} + A_4 e^{-i\nu t} \\ &= A_1 e^{\lambda t} + A_2 e^{-\lambda t} + C_1 \cos \nu t - C_2 \sin \nu t \end{aligned} \quad (47)$$

The behaviour of x depends on the sign of A_1 and A_2 , such that for each energy level 4 cases can be identified near the collinear libration points (L_1 , L_2 and L_3) [Conley, 1967]:

1. $A_1 = A_2 = 0$: The periodic solution (Lyapunov orbit)
With the semi-major axis (in y-direction) $a = \sqrt{\tau^2 x_0^2 + y_0^2}$ and the semi-minor axis (in x-direction) $b = \sqrt{x_0^2 + \frac{y_0^2}{\tau^2}}$.

2. $A_1 A_2 = 0$: Orbits that are asymptotic to the periodic orbit, approaching it or moving away.
3. $A_1 A_2 < 0$: Orbits that cross the equilibrium region and are therefore called 'transit'.
4. $A_1 A_2 > 0$: Orbits that are called 'non-transit'.

These classes of orbits are shown in Figure 13 and indicated with B, A, T and NT respectively.

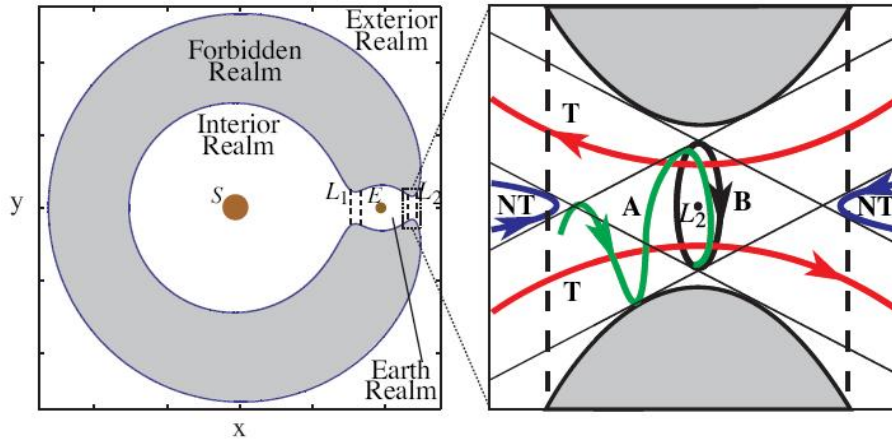


Figure 13: The different classes of orbits in the equilibrium region [Koon, 2006].

Analysis of the phase-space flow in the equilibrium regions [Gomez, 2001] shows that the asymptotic orbits are part of the stable and unstable manifold tubes of the periodic orbit. These tubes are separatrices for the transit and non-transit orbits. The transit orbits are inside the manifold tubes, such that they can transport material or better a spacecraft from and to the smaller massive body and between separate three-body models, as shown in Figure 14. The theory can also be extended to the three-dimensional case, and two three-body systems can be coupled.

4.3 Extension to the spatial case and 4-body problem

When also latitude and longitude of the spacecraft become important for the design of a trajectory, the spatial circular restricted 3-body problem should be considered. The equation of motion in the z -direction is decoupled of the other two and can be linearized to [Wakker, 2007a]:

$$\ddot{z} = U_{zz}\dot{z} \quad (48)$$

Its solution is a stable and purely periodic motion:

$$z = C_1 \cos(\sqrt{|U_{zz}|}t) + C_2 \sin(\sqrt{|U_{zz}|}t) \quad (49)$$

Because the Poincaré cut is a 3-sphere and both in the y, \dot{y} and the z, \dot{z} projections it is a 2-dimensional disc, it is hard to find intersections. Therefore constraints

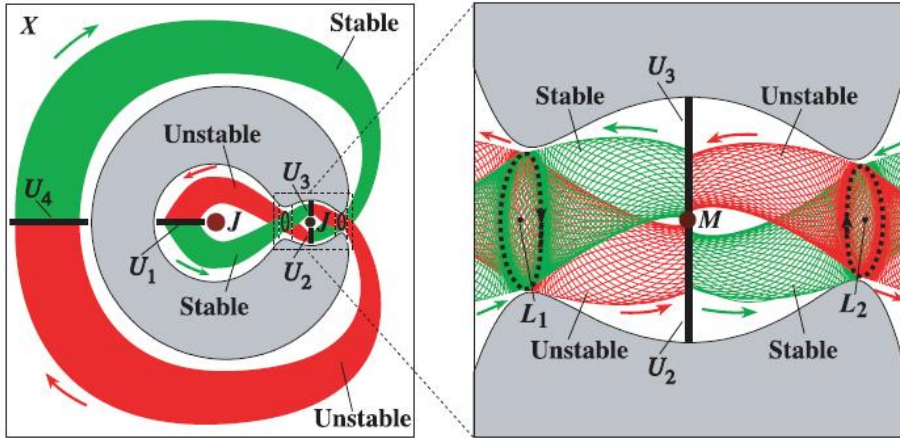


Figure 14: Libration point invariant manifolds in position space (U_i are Poincaré cuts) [Gomez, 2004].

on z and \dot{z} are proposed, for example:

$$\begin{aligned} z &= c \\ \dot{z} &= 0 \end{aligned} \quad (50)$$

Now the set of orbits in the Poincaré cut of the unstable manifold with these constraints (a point in the z, \dot{z} -plane) projects to a curve on the y, \dot{y} -plane. Any point which is inside this curve is a transit orbit from the exterior region through R. Similarly this can be done for the Poincaré-cut of the stable manifold through R to the interior region. Now the points can be extended to boxes $z \pm \delta z, \dot{z} \pm \delta \dot{z}$ [Gomez, 2004]. Then the curve in the y, \dot{y} -plane becomes a strip (Figure 15).

How to compute the manifolds and trajectories exactly, is subject of Chapter 6 and further.

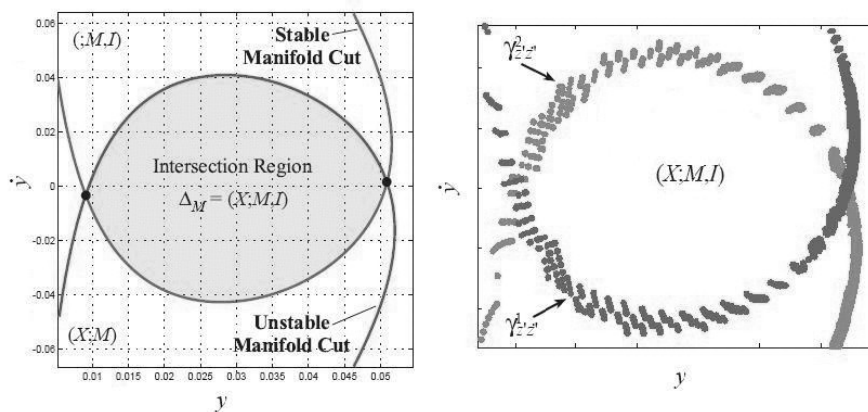


Figure 15: Examples of Poincaré sections of manifolds in y, \dot{y} -plane for the planar (left) and spatial case (right) [Gomez, 2001].

The spatial model is also needed when coupling two 3-body models which are not in the same plane. This patched three-body approximation [Koon, 2006] couples two systems with only one massive body changed; like for example Earth-Sun-spacecraft and Earth-Moon-spacecraft (*bicircular model*) or Earth-Sun-spacecraft and Mars-Sun-spacecraft (*concentric circular model*). Both versions of the PCR4BP are shown in Figure 16. Equivalently to the patched conics approach for two-body motion in the n-body problem, the 4-body problem now is approximated by two segments of purely 3-body motion. The initial solution (existing of a stable manifold-unstable manifold trajectory) is then refined in the full 4-body problem, such that the ephemeris of the motion of the planets and moons can be taken into account.

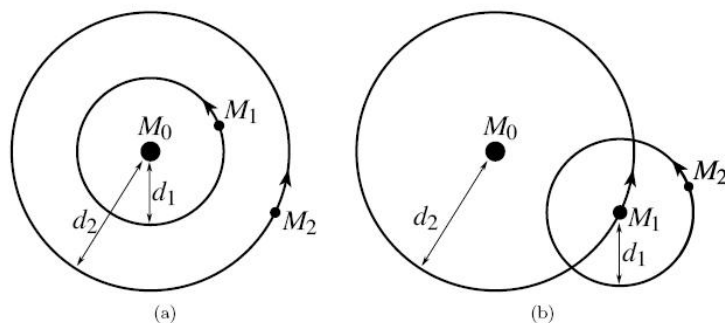


Figure 16: (a) The concentric circular model (b) The bi-circular model [Koon, 2006].

The determination of periodic orbits in the non-linearized case is discussed in the next chapter, the generation of manifolds in Chapter 6 and the coupled CR3BP in Chapter 7.

5 Periodic orbits

Periodic orbits about the libration points serve as a starting point for the connections. The positions of the libration points can be determined when the planets involved are known (Table 2). Also the appropriate energy level can be selected (Figure 8), such that the neck between the inner and exterior region exists in the Hill surfaces. In this section only planar periodic orbits or Lyapunov orbits are discussed. The theory however also applies to the spatial case and halo orbits.

5.1 Differential correction

The periodic orbit as given in Section 4.2 is only valid for the linearized system and serves as an initial guess in the full system. It should be adjusted by means of differential correction. Differential correction is used to adjust an initial condition x_0 in order to reach a desired target point x_d at time t_1 [Howell, 1988]. In practice it is an iterative scheme to reduce discontinuities in position and/or velocity to zero.

Therefore the State Transition Matrix (STM) is needed [Koon, 2006]. It relates small initial displacements to displacements in the final state:

$$\delta\bar{x}(t_1) = \Phi(t_1, t_0)\delta\bar{x}_0 \quad (51)$$

It can be found via integration of the set of initial conditions and $(n^2 + n)$ differential equations [Kumar, 2008]:

$$\begin{aligned} \bar{x}(t_0) &= \bar{x}_0 \\ \dot{\bar{x}} &= f(\bar{x}) \\ \Phi(t_1, t_0) &= I_{n \times n} \\ \dot{\Phi}(t, t_0) &= F\Phi(t, t_0) \end{aligned} \quad (52)$$

In this case the function $f(\bar{x})$ are the equations of motion and the vector \bar{x} is the state vector $(x \ y \ \dot{x} \ \dot{y})^T$. Based on the linearized equations of motion in Equation 39, the matrix F is found to be:

$$F = \begin{bmatrix} 0 & I \\ U_{xx} & 2A \end{bmatrix} \quad (53)$$

In the case of planar motion ($n = 4$) every input is a 2 by 2 matrix; U_{xx} is the full array of second-order partial derivatives of U (Equation 43) and A is defined as:

$$A = \begin{bmatrix} 0 & 1 \\ -1 & 0 \end{bmatrix} \quad (54)$$

The planar periodic orbit is symmetric with respect to the x-axis ($y = 0$) and intersects it perpendicularly ($\dot{x} = 0$) [Broucke, 1973]. So the initial and final states should be of the form:

$$\bar{x}_i = (x_i \ 0 \ 0 \ \dot{y}_i)^T \quad (55)$$

Now the initial state can be integrated forward by means of the non-linear equations of motion until the first crossing with the x-axis, which is when y

changes sign. The time now is defined as $\frac{T}{2}$, such that the periodic orbit will have period T . Probably the first attempt will give \dot{x}_1 not equal or close enough to zero, so the initial state is to be changed to:

$$\bar{x}_0 = (\delta x_0 \quad 0 \quad 0 \quad \delta \dot{y}_0)^T \quad (56)$$

such that the desired change in final state is $\delta \dot{x}_1 = -\dot{x}_1$. Based on a Taylor expansion the change in state is defined as:

$$\delta \bar{x} = \Phi\left(\frac{T}{2}, t_0\right)\delta \bar{x}_0 + \frac{\delta \bar{x}}{\delta t}\delta\left(\frac{T}{2}\right) \quad (57)$$

Now the corrections can be computed by keeping x_0 constant via:

$$\delta \dot{x}_1 = \Phi_{34}\delta \dot{y}_0 + \ddot{x}_1\delta\left(\frac{T}{2}\right) = \left(\Phi_{34} - \frac{\ddot{x}_1}{\dot{y}_1}\Phi_{24}\right)\delta \dot{y}_0 \quad (58)$$

Here Φ_{ij} is the j 'th entry on the i 'th row of the STM. Only a few iterations are needed to find the periodic orbit [Howell, 1984].

Because this is based on the linearization around the libration points, this method will deliver only small-amplitude periodic orbits. The amplitude is related to the level of energy. Numerical continuation can generate families of orbits with larger amplitudes, which reaches the appropriate energy [Koon, 2006].

Suppose two periodic orbits with initial conditions $\bar{x}_{0,1}$ and $\bar{x}_{0,2}$ are found by differential correction. Then a third initial state can be found by extrapolation:

$$\Delta = \bar{x}_{0,2} - \bar{x}_{0,1} = (\Delta x_0, 0, 0, \Delta \dot{y}_0)^T \quad (59)$$

$$\bar{x}_{0,3} = \bar{x}_{0,2} + \Delta \quad (60)$$

Again differential correction can be applied and this process can be repeated to generate a family of periodic orbits. Keeping track of the energy levels of each orbit, the two initial states used for extrapolation can be chosen such that it refines towards the appropriate energy level for the design of a trajectory.

5.2 Results and verification

The generation of periodic orbits in Tudat requires only input of mass parameter μ , initial position x_0 and energy constant C . The value for \dot{y}_0 follows from these values and Equation 23.

Due to the correction in \dot{y} , the energy levels of the periodic orbit differ slightly from the initial ones. The choice of initial value for C , as long as a periodic orbit is obtained, seems to have little influence on the corrected initial conditions. This is shown in Table 3 for a μ of the Sun-Earth system and an initial position of 1.008. The position is closest to the L_2 libration point (at $x = 1.01003$), which has an energy of 3.00089. For comparison the amplitudes A in both directions and the period of the Lyapunov orbit T are computed, all in normalized units.

Visualizing these orbits (Figure 17) however shows that only one orbit (the one with $C_0 = 3.0008$) is truly about the libration point. Which means that an

obtained periodic orbit can only be validated after visual inspection. A quick check should include that periodic orbits about the collinear libration points have smaller amplitudes in x than in y direction [Wakker, 2007a]. This fact can be used in automating the grid search for the right initial conditions.

In Table 4 and Figure 18 the same analysis is performed for a variety of initial positions x_0 and a constant $C_0 = 3.0008$. It shows that the periodic orbit and its energy level are very sensitive to changes in initial position. Therefore both C_0 and x_0 should be chosen close to the energy level and position of the libration point and the periodic orbit should be examined first. Otherwise a consequence might be that not an orbit about the libration point, but about the planet is obtained. A study to the effects on the generation of L_1 Lyapunov orbits shows similar behaviour (not depicted here).

For small μ , as is the case in this study (Table 2, $\mu < 10^{-4}$), the different cases as defined for the Hill-surfaces and their energy levels (Figure 8) are very close together. However, continuation or correction of the initial x_0 will only be meaningful when other limits on the energy level are imposed, as is done in Chapter 7. Then the energy level will be fixed and the initial position will be manually adjusted using a simple grid search until the orbit converges to a periodic orbit appropriate for the given problem.

C_0 [-]	C [-]	A_x [-]	A_y [-]	T [-]
3.0000	No convergence			
3.0001	3.0008816	0.004738	0.003752	1.959
3.0005	3.0008814	0.004728	0.003731	1.961
3.0007	3.0008812	0.004719	0.003709	1.964
3.0008	3.0007902	0.001827	0.005407	3.125
3.00085	3.0008813	0.004722	0.003722	1.964
3.0009	3.0008812	0.004718	0.003708	1.964
3.001	No convergence			
3.005	No convergence			

Table 3: Effect of initial energy level C_0 on generation of planar periodic orbits and their amplitudes A and period T , via Tudat. Mass parameter μ is equal to $3.0043 \cdot 10^{-6}$ (i.e. Sun-Sarth system) and $x_0 = 1.008$.

In literature [Broucke, 1968] the data of a total of 10 periodic orbits in the Earth-Moon system ($\mu = 0.012155092$) are available. In this system the libration points L_1 and L_2 are located at 0.8369 and 1.1157 with energy levels 3.1884 and 3.1722, respectively. Using differential correction as implemented in Tudat, the same orbits are generated. A comparison of results (in Tables 5 and 6), shows close resemblance for case 1 to 9. Only for exotic cases like case 10 (low C , x far from libration point) discrepancies may show, because of multiple x -axis crossings. Some examples of the orbits used for this comparison are shown in Figures 19 and 20, from which the same conclusions can be drawn.

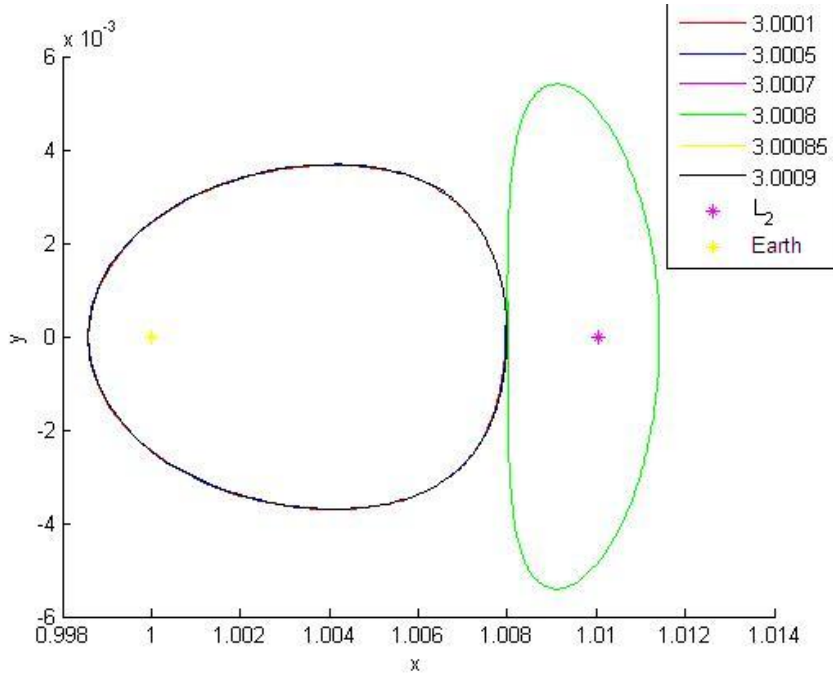


Figure 17: Effect of initial energy level C_0 on generation of planar periodic orbits, via Tudat. Mass parameter μ is equal to $3.0043 \cdot 10^{-6}$ (i.e. Sun-Sarth system) and $x_0 = 1.008$.

x_0 [-]	C [-]	A_x [-]	A_y [-]	T [-]
1.000	No convergence			
1.005	3.00092	0.00416	0.004459	1.263
1.008	3.0007902	0.001827	0.005407	3.125
1.009	3.0008573	0.0009353	0.002974	3.075
1.01	2.9999659	0.009992	0.01245	2.675
1.05	3.005712	0.2165	0.4752	37.73
1.1	3.01747	0.4309	0.6358	25.14
1.2	3.07363	1.26	0.9078	12.57

Table 4: Effect of initial position x_0 on generation of planar periodic orbits and their amplitudes A and period T , via Tudat. Mass parameter μ is equal to $3.0043 \cdot 10^{-6}$ (i.e. Sun-Sarth system) and $C_0 = 3.0008$.

As a conclusion, the generation of Lyapunov orbits about the L_1 and L_2 libration points is strongly dependent on the choice of initial energy level and position. However, after adjustment of the initial parameters and visual examination of the obtained orbit, these planar periodic orbit can be accurately computed with Tudat and may serve as a starting point for the design of a trajectory by means of DST.

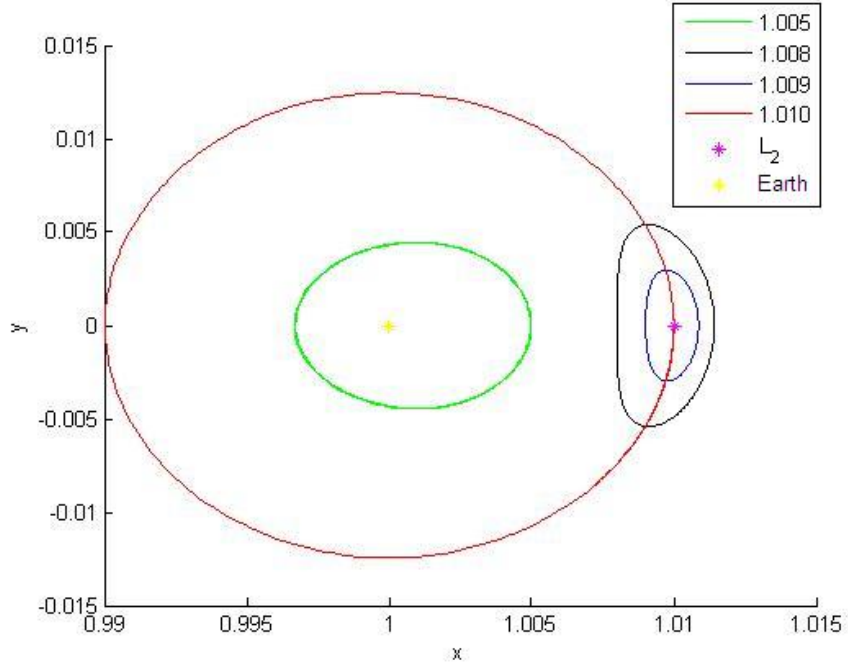


Figure 18: Effect of initial position x_0 on generation of planar periodic orbits, via Tudat. Mass parameter μ is equal to $3.0043 \cdot 10^{-6}$ (i.e. Sun-Sarth system) and $C_0 = 3.0008$.

case	$x_0[-]$	Reference			Tudat		
		$\dot{y}_0[-]$	$C[-]$	$T[-]$	$\dot{y}_0[-]$	$C[-]$	$T[-]$
1	0.809282	0.281940	3.11689	3.01649	0.279377	3.11819	3.0090
2	0.804226	0.325927	3.09300	3.17330	0.325925	3.09301	3.1734
3	0.741687	0.546776	2.97072	5.02655	0.546759	2.97074	5.0272
4	0.668848	0.708265	2.92307	6.28319	0.708264	2.92308	6.2832
5	0.050000	5.458020	2.02492	6.82793	5.458010	2.02501	6.8280

Table 5: Lyapunov periodic orbits around the Earth-Moon L_1 , via Tudat and [Broucke, 1968].

case	$x_0[-]$	Reference			Tudat		
		$\dot{y}_0[-]$	$C[-]$	$T[-]$	$\dot{y}_0[-]$	$C[-]$	$T[-]$
6	1.18971	-0.225810	3.12870	3.47867	-0.225809	3.12870	3.47880
7	1.21610	-0.414022	3.02252	4.18719	-0.414020	3.02253	4.18720
8	1.30352	-0.581492	2.93970	6.28318	-0.581482	2.93971	6.28320
9	1.69366	-1.141870	2.75728	9.42476	-1.141870	2.75728	9.42480
10	2.44861	-1.907590	2.29519	10.6814	-1.809770	3.53994	8.50698

Table 6: Lyapunov periodic orbits around the Earth-Moon L_2 , via Tudat and [Broucke, 1968].

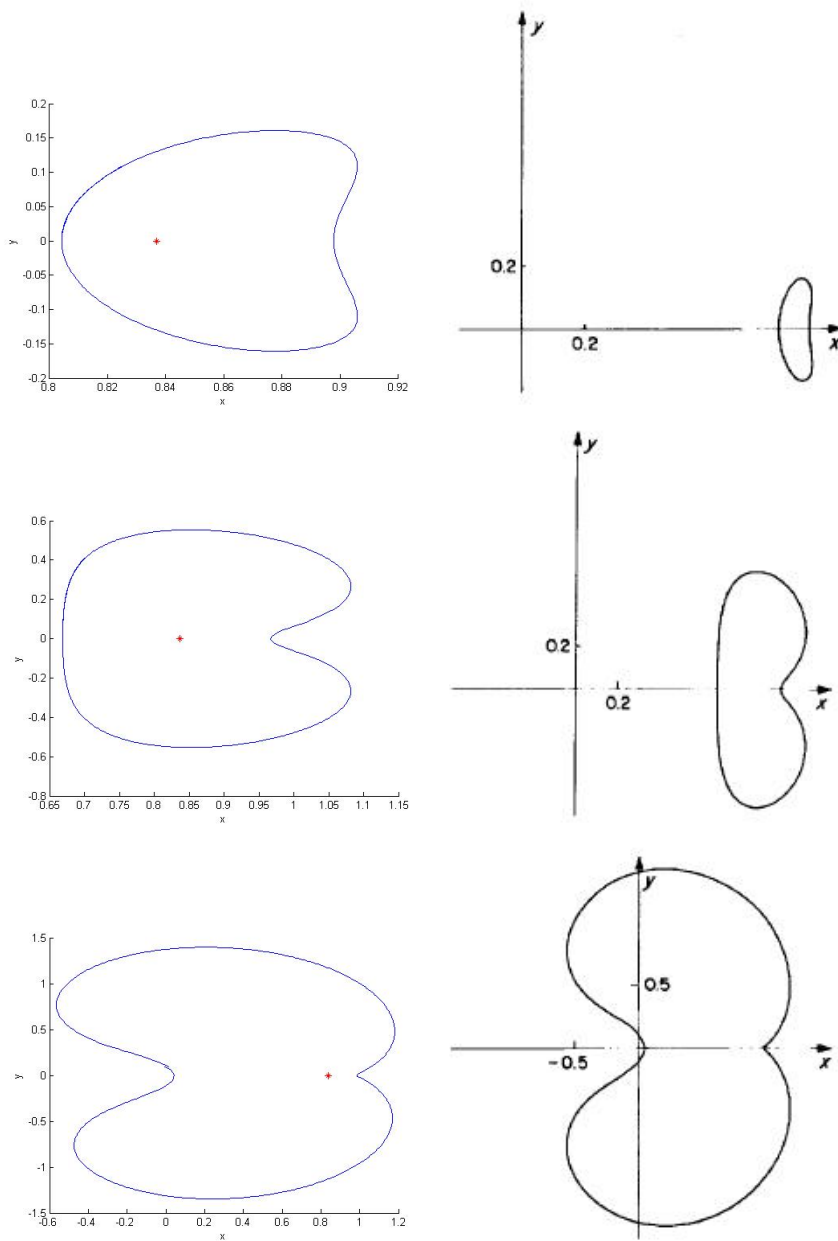


Figure 19: Orbits 2, 4 and 5 about the Earth-Moon L_1 , via Tudat (left) and [Broucke,1968] (right).

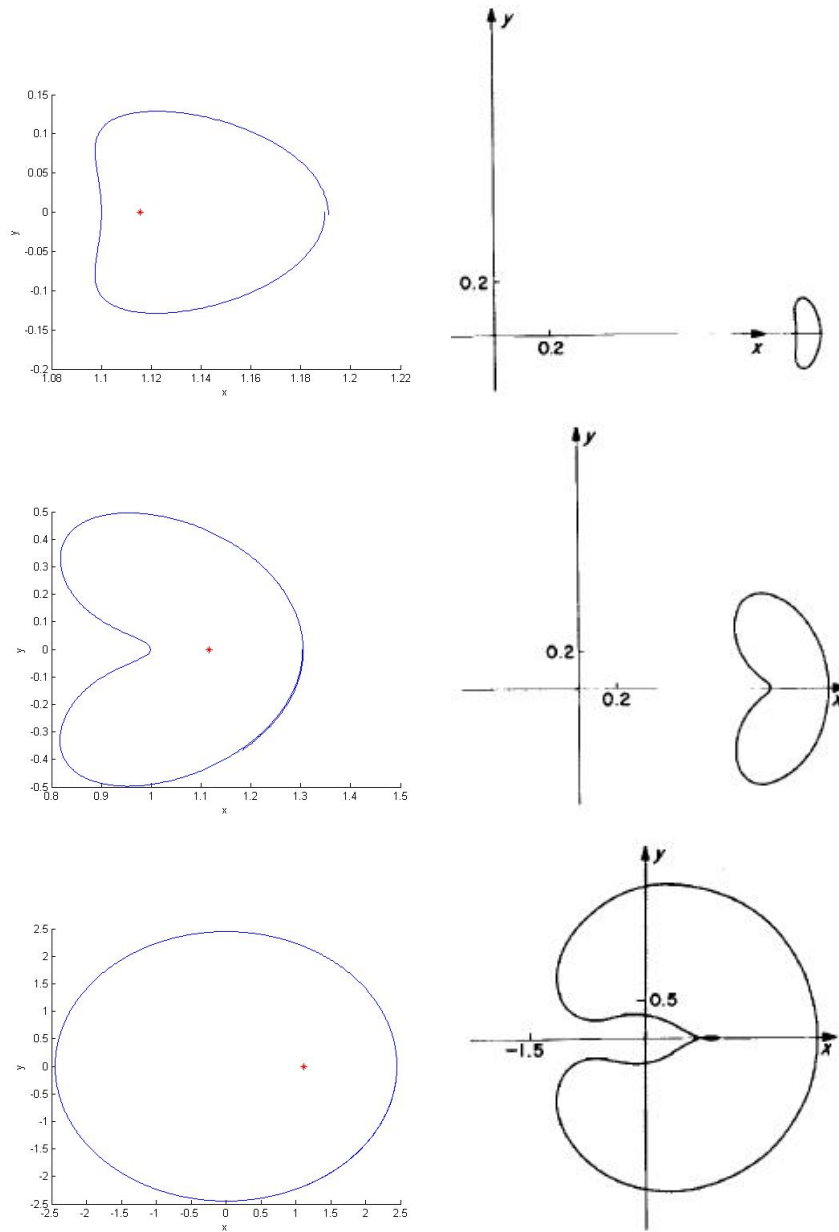


Figure 20: Orbits 6, 8 and 10 about the Earth-Moon L_2 , via Tudat (left) and [Broucke,1968] (right).

6 Manifolds

Manifolds emanating from the periodic orbits are candidates for paths for interplanetary transfer. Simulation of large families of orbits, may result in the manifold tubes as presented in Section 4. For comparison, this part of the design is also performed with AUTO-07p. The theoretical background and use of this tool is discussed in more detail in Appendix C.

6.1 Generation of manifolds

Manifolds are computed by integration of a large number of orbits forward (unstable) or backward (stable) in time from initial conditions given by displacing the spacecraft a small distance d from the periodic orbit.

The monodromy matrix is the STM after one revolution (so $t = t_0 + T$). Its first two eigenvalues (which are real) correspond to the directions of the unstable and stable manifold respectively [Guzman, 1998]. With their normalized eigenvectors \bar{v} , for every starting point x_0 on the periodic orbit, a manifold can be computed via:

$$\begin{aligned} W_u(x_0) &= x_0 \pm d\bar{v}_1(x_0) \\ W_s(x_0) &= x_0 \pm d\bar{v}_2(x_0) \end{aligned} \quad (61)$$

The distance d must be small enough such that the linearization is valid and large enough such that one can get somewhere in a reasonable amount of time. Ultimately, manifolds are computed by combining trajectories obtained from a large number of initial points x_0 on the periodic orbit.

The local eigenvectors can be found by integrating forward the STM [James, 2006] until reaching the initial point on the periodic orbit:

$$\bar{v}(x_0) = \Phi(0, t_0)\bar{v}(0) \quad (62)$$

6.2 Results from Tudat

In Figure 21 the Lyapunov orbits and 100 starting points for a mass parameter $9.53678 \cdot 10^{-4}$ (Sun-Jupiter system) are visualized. The initial condition for the orbits about the L_1 and L_2 libration point respectively are $C = 3.0274$, $x_0 = 0.92$ and $C = 3.032$, $x_0 = 1.08$. Both the periodic orbits and the initial points are obtained using Tudat. Again, the starting points are obtained by adding the eigenvectors scaled with the deviation parameter d to 100 equally spaced (in time) points on these periodic orbits (Equation 61).

When integrating respectively backwards and forwards for a fixed amount of time ($t = \frac{5}{2\pi}$) and plotting every resulting second manifold, the structure of the manifolds shows in Figures 22 and 23. These figures are all in normalized units and the system's rotating reference frame. The shape of the figures show great resemblance with the ones generated using AUTO (not depicted).

The deviation parameter (d in Equation 61) can be adjusted, such that the initial points will shift. This is done for the L_2 periodic orbit for deviations of 10^{-3} , 10^{-4} , 10^{-6} and 10^{-8} , while in Figure 21 a deviation of 0.01 was used.

The effect of smaller deviations on the resulting manifolds is shown in Figure 24. The initials points will approach the periodic orbit for smaller deviations.

For the same amount of integration time, the entire manifold structure becomes shorter and smaller, because some of the manifolds never leave the vicinity of the periodic orbit and other will take longer to do so. This means that the deviation should be chosen as large as possible, without loss of accuracy. A quick check for this type of accuracy is the examination of the manifolds energy levels.

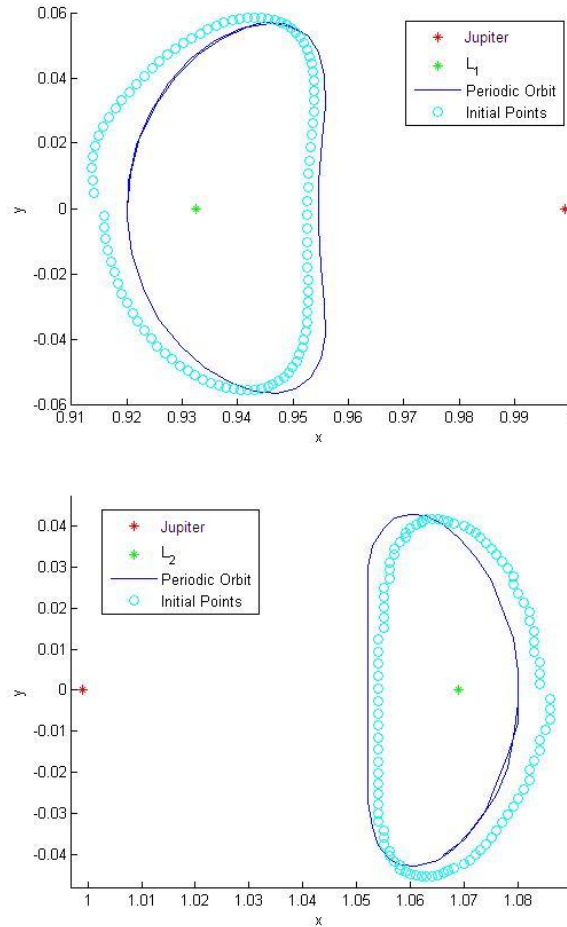


Figure 21: Periodic orbits and initials points (for $d = 0.01$) in the Sun-Jupiter system, generated via Tudat.

Along orbits on a manifold the Jacobian energy constant (Equation 23) should be constant. For the computed orbits of Figures 22 and 23 (with deviation $d = 0.01$) this is the case, however a range of energy levels along the manifolds can be witnessed. The mean energy of the L_1 manifold is 3.0276 and its standard deviation $8.7159 \cdot 10^{-4}$. For the L_2 manifold and the different deviations from the periodic orbit, these statistics are shown in Table 7. Based on this, for this specific problem a deviation d of 10^{-3} should be chosen to scale the eigenvector with. When generating manifolds in other Sun-planet systems or emanating from other periodic orbits, the same test will be used.

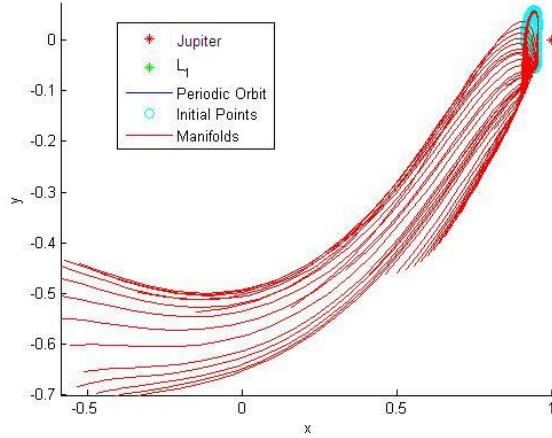


Figure 22: L_1 manifold in the Sun-Jupiter system, generated via Tudat.

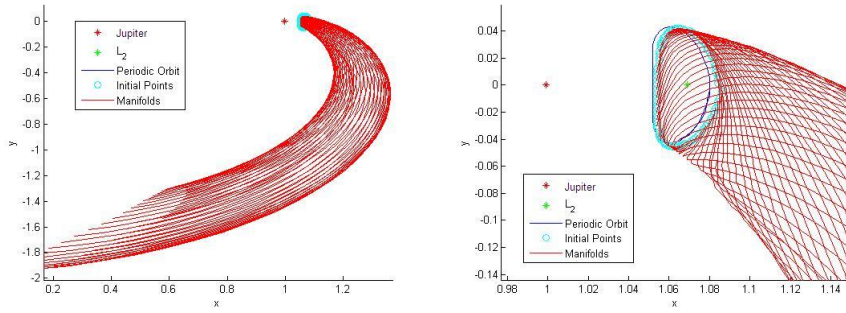


Figure 23: L_2 manifold in the Sun-Jupiter system, generated via Tudat.

d [-]	C mean [-]	C std [-]
10^{-1}	3.0319	$4.2 \cdot 10^{-3}$
10^{-2}	3.032	$1.4003 \cdot 10^{-4}$
10^{-3}	3.032	$1.0349 \cdot 10^{-13}$
10^{-4}	3.0319	$1.2437 \cdot 10^{-13}$
10^{-6}	3.032	$1.0349 \cdot 10^{-13}$
10^{-8}	3.032	$1.0349 \cdot 10^{-13}$

Table 7: Effect of deviation d from the periodic orbit on the accuracy of the L_2 manifold in the Sun-Jupiter system, generated via Tudat.

6.3 Verification and comparison

Other implementations of the presented theory can be used for comparison. For the Sun-Earth system [Herman, 2012], has found a periodic orbit, the stable eigenvector and the end points of a certain manifold. This dataset has been used as a unit test to verify the code in Tudat. The results are shown in Table 8. The initial conditions of the planar periodic orbit about L_1 were $x = 0.98883$

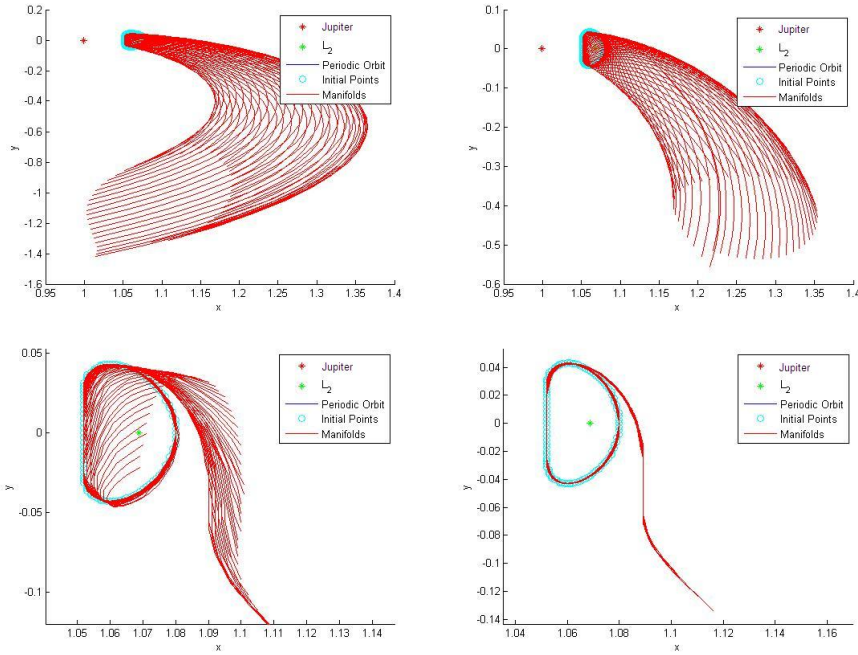


Figure 24: L_2 manifold in the Sun-Jupiter system (a. $d=10^{-3}$ b. $d=10^{-4}$ c. $d=10^{-6}$ d. $d=10^{-8}$), generated via Tudat.

and $\dot{y} = 0.00883$ and a deviation from this periodic orbit of 10^{-6} was used. The end points are determined after 10 times the period of the periodic orbit, $T_{end} = 30.60155$. The direction of the eigenvector (positive or negative) can be chosen as preferred, as shown in Figure 13 and Equation 61.

The results obtained with the RK4 and RKF78 integrators (Appendix A) are equal for computer accuracy (10^{-10}) and may serve as verification of the accuracy of both integration techniques and their implementation in Tudat for this specific problem.

	Tudat		Reference	
	eigenvector	final state	eigenvector	final state
x [-]	-0.36309	-0.35096	0.36309	-0.35096
y [-]	0.12255	0.85664	-0.12255	0.85664
\dot{x} [-]	-0.83726	-0.12067	0.83726	-0.12067
\dot{y} [-]	0.39006	-0.04510	-0.39006	-0.04510

Table 8: Comparison of eigenvectors of a Sun-Earth L_1 manifold and its final state after integration over T_{end} , from Tudat and from [Herman, 2012].

The results in this chapter show that with the theory presented and implemented in Tudat, the manifolds emanating from the periodic orbits can easily and accurately be generated. Next the manifolds from different Sun-planet systems are to be generated and connected for interplanetary transfer.

7 Coupling two planar CR3BP's

Because of the almost planar motion of planets in our solar system, a first analysis of manifolds in this system is performed in the planar CR3BP (PCR3BP). Coupling two of such systems, typically the possibilities for transfer from one Sun-planet system to another can be investigated.

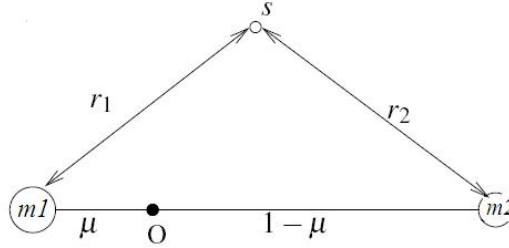


Figure 25: Position vectors in normalized units and rotating reference frame in the PCR3BP [Calleja, 2011].

7.1 Coupled 3-body systems

Converting the obtained state vectors back to standard units and using the rotation of the planets in their circular coplanar orbits, the trajectories in separate three-body systems can be expressed with respect to a common inertial reference frame, and ideally be coupled. An example of such a conversion is shown in Figure 26, for the unstable manifolds emanating from a periodic orbit about the Sun-Jupiter's L_2 libration point.

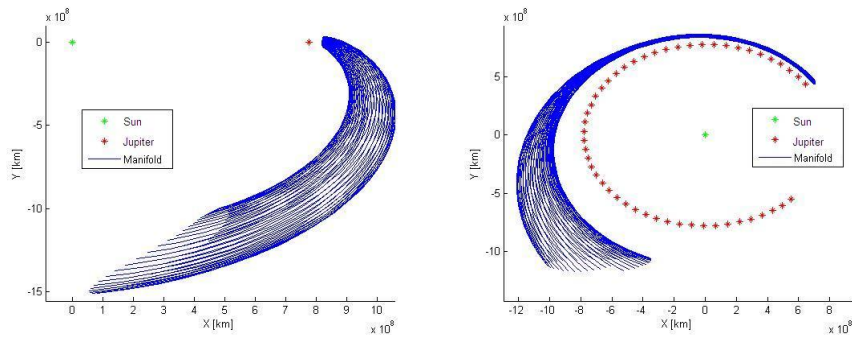


Figure 26: L_2 unstable manifold in the Sun-Jupiter system (a. Rotating reference frame b. Inertial reference frame), generated via Tudat.

As described in Chapter 2, distance was normalized to the distance between the two massive bodies and velocity to the rotational speed of the system. So, multiplication of the normalized vectors with these two scalars, will yield position and velocity in meters and meters per second respectively. Time was normalized

to one over the mean motion, so:

$$\begin{aligned} X &= R_{12}x \\ V &= V_{12}v = R_{12}\omega_{12}v \\ T &= \frac{1}{\omega_{12}}t \end{aligned} \quad (63)$$

In these equations, the lower-case symbols represent normalized parameters, whereas the upper-case parameters are in standard units. The Jacobian energy constant in standard units in a reference frame rotating with mean motion ω_{12} is given by:

$$\omega_{12}^2 (X^2 + Y^2) + 2 \left(\frac{Gm_1}{R_1} + \frac{Gm_2}{R_2} \right) - V^2 \quad (64)$$

As shown in Figure 25, the positions of m_1 (OP_1) and m_2 (OP_2) have been normalized to μ and $1 - \mu$ respectively. From theoretical mechanics it is known that if m_2 (and thus also m_1) moves in a circular orbit, the motion of m_2 is given by:

$$\begin{aligned} m_2\omega_{12}^2 OP_2 &= \frac{Gm_1 m_2}{R_{12}^2} \\ \omega_{12}^2 OP_2 &= \frac{Gm_1}{R_{12}^2} \\ \omega_{12}^2 R_{12}(1 - \mu) &= \frac{Gm_1}{R_{12}^2} \\ \omega_{12}^2 R_{12}^2(1 - \mu) &= \frac{Gm_1}{R_{12}} \\ \omega_{12}^2 R_{12}^2 \frac{1 - \mu}{r_1} &= \frac{Gm_1}{R_{12}r_1} \\ \omega_{12}^2 R_{12}^2 \frac{1 - \mu}{r_1} &= \frac{Gm_1}{R_1} \end{aligned} \quad (65)$$

In the same way:

$$\omega_{12}^2 R_{12}^2 \frac{\mu}{r_2} = \frac{Gm_2}{R_2} \quad (66)$$

such that Equation 64 becomes:

$$\begin{aligned} \omega_{12}^2 ((R_{12}x)^2 + (R_{12}y)^2) + 2 \left(\omega_{12}^2 R_{12}^2 \frac{1 - \mu}{r_1} + \omega_{12}^2 R_{12}^2 \frac{\mu}{r_2} \right) - (R_{12}\omega_{12}v)^2 \\ = \omega_{12}^2 R_{12}^2 \left[(x^2 + y^2) + 2 \left(\frac{1 - \mu}{r_1} + \frac{\mu}{r_2} \right) - v^2 \right] \end{aligned} \quad (67)$$

which means that the normalized Jacobian energy (Equation 23) may be converted to SI units directly via:

$$C = \omega_{12}^2 R_{12}^2 c = V_{12}^2 c \quad (68)$$

In the case of a Sun-planet system, the rotational speed of the system V_{12} is the velocity of the planet rotating about the Sun.

The energy level is defined as $E = -\frac{1}{2}C$ or via:

$$E_{rot} = \frac{1}{2}V^2 - \left(\frac{Gm_{Sun}}{R_1} + \frac{Gm_{planet}}{R_2} \right) - \frac{1}{2}\omega_{12}^2 (X^2 + Y^2) \quad (69)$$

In an inertial reference frame the correction for the rotating system is missing and the energy only consists of the sum of kinetic and potential energy [Wakker, 2007]:

$$E_{in} = \frac{1}{2}V_{in}^2 - \left(\frac{Gm_{Sun}}{R_1} + \frac{Gm_{planet}}{R_2} \right) \quad (70)$$

The velocity in an inertial reference frame is defined as:

$$V_{in} = V_{rot} + \bar{\Omega} \times \bar{R} = V_{rot} + [0 \ 0 \ \omega_{12}]^T \times [X \ Y \ 0]^T = V_{rot} + \omega_{12}[-Y \ X \ 0]^T \quad (71)$$

For the orbits of the planets, the initial J2000 ephemeris of [Standish, 2011] is used. The semi-major axis is assumed constant and the mean longitude (defined for circular orbits) will change according to the given initial value and change rate.

With the presented conversions the energy levels within two different CR3BP's can be compared and the manifold tubes can be visualized in one figure.

7.2 Analysis of energy levels

The minimum energy levels are based on analysis of the Hill surfaces (Figure 7); they should just allow for transfer from and to the area around the libration points. For the stable manifold from L_1 the inner region should be accessible, which results in C_{L_1} , and for the unstable manifold from L_2 the outer region is to be accessed, resulting in C_{L_2} .

Using the location of the libration points (Table 2) and Equation 23, the values of these specific energy levels can be computed. For both libration points they are shown in Table 9 in normalized units for each particular planet-Sun system. In [Elvik, 2004] values for these energy levels from AUTO were found, which serve as a reference. For comparison the energy levels are also given in standard units (Equation 68) and with respect to an inertial reference frame (Equation 70) in Table 10. Note that the inertial velocity (Equation 71) of a collinear libration point ($V = 0$ and $Y = 0$) becomes:

$$\begin{aligned} V_{in} &= \omega_{12}[0 \ X_L \ 0]^T \\ V_{in}^2 &= \omega_{12}^2 X_L^2 = \omega_{12}^2 (R_{12} x_L)^2 = V_{12}^2 x_L^2 \end{aligned} \quad (72)$$

For the generation of manifolds the software uses the normalized energy constants C (Table 9), while for analysis the physical interpretable energy levels E (Table 10) are more suitable.

Planet	Tudat		AUTO	
	$C_{L_1}[-]$	$C_{L_2}[-]$	$C_{L_1}[-]$	$C_{L_2}[-]$
Mercury	3.00013	3.00013	3.000130	3.000130
Venus	3.00078	3.00077	3.000777	3.000774
Earth	3.00089	3.00089	3.000891	3.000886
Mars	3.00020	3.00020	3.000202	3.000202
Jupiter	3.03876	3.03748	3.038756	3.037483
Saturn	3.01782	3.01744	3.017822	3.017440
Uranus	3.00522	3.00516	3.005219	3.005161
Neptune	3.00582	3.00575	3.005817	3.005749

Table 9: Minimum normalized energy levels for transfer through the area around libration points, via Tudat and AUTO.

Increasing these energy levels (decreasing the Jacobian energy constant C) results in more possibilities for transfer, but also a larger energy demand in

Planet	Rotating frame				Inertial frame	
	C_{L_1} [km^2s^{-2}]	C_{L_2} [km^2s^{-2}]	E_{L_1} [km^2s^{-2}]	E_{L_2} [km^2s^{-2}]	E_{L_1} [km^2s^{-2}]	E_{L_2} [km^2s^{-2}]
Mercury	5512.14	5512.13	-2756.07	-2756.07	-1163.41	-1128.48
Venus	3737.04	3737.03	-1868.52	-1868.52	-636.44	-590.60
Earth	2689.04	2689.03	-1344.52	-1344.52	-461.56	-426.06
Mars	1479.32	1479.32	-739.66	-739.66	-296.69	-285.61
Jupiter	516.16	515.95	-258.08	-257.98	-110.86	-64.15
Saturn	310.48	310.44	-155.24	-155.22	-55.31	-38.37
Uranus	126.22	126.22	-63.11	-63.11	-25.40	-20.89
Neptune	90.19	90.19	-45.10	-45.10	-16.31	-13.27

Table 10: Minimum standard energy levels for transfer through the area around libration points, computed using Tudat.

terms of velocity increments ΔV . The two increments are related due to Equation 23.

As the Jacobian energy constant C is the integral of motion in the PCR3BP, it remains constant along a manifold. So the possibilities for transfer are also limited by the energy gap between the unstable and stable manifolds of two different planet-Sun systems. In some cases this energy gap might be overcome using a planetary swing by, which reduces the needed velocity increments. The planet in the system of departure can be used as swing-by planet, when utilizing a connection in the planetary region as shown in for example Figure 12. In Figure 27 the maximum energy increments reachable by means of a swing-by are shown; more realistic values can be computed according to the theory in Section 2.3 and are to be converted back to C .

The maximum energy levels are limited due to the stability of the Lyapunov periodic orbits. With the family of periodic orbits generated in AUTO (as shown in Figure 28), the energy level of the outermost periodic orbit is assumed to be the maximum energy level. It corresponds to the orbit which causes collision with the primary body and therefore the continuation is terminated naturally. The energy levels with respect to a rotating reference frame are constant over the orbit as long as the satellite is kept far enough ($0.1R_{12}$ is used) from collision. These values are given in Table 11 for every Sun-planet system.

Also the minimum values have been checked by inspecting the values of C and E for the innermost periodic orbit, being the libration point itself; the results are consistent.

In Table 12 the minimum energy levels (of Table 10) and maximum swing-by energy increments (based on Figure 27), are summarized. Also the energy gap between one planet's L_2 energy level to the next planet's L_1 energy level are given. Although the inertial energy levels are not completely constant, it is likely that transfer is only possible for small differences in energy. When considering transfer from one planet's L_2 point to the following planet's L_1 point, with a possible swing-by at the first planet, the only options for transfer worth investigating are Earth-Mars, Jupiter-Saturn, Saturn-Uranus and Uranus-Neptune.

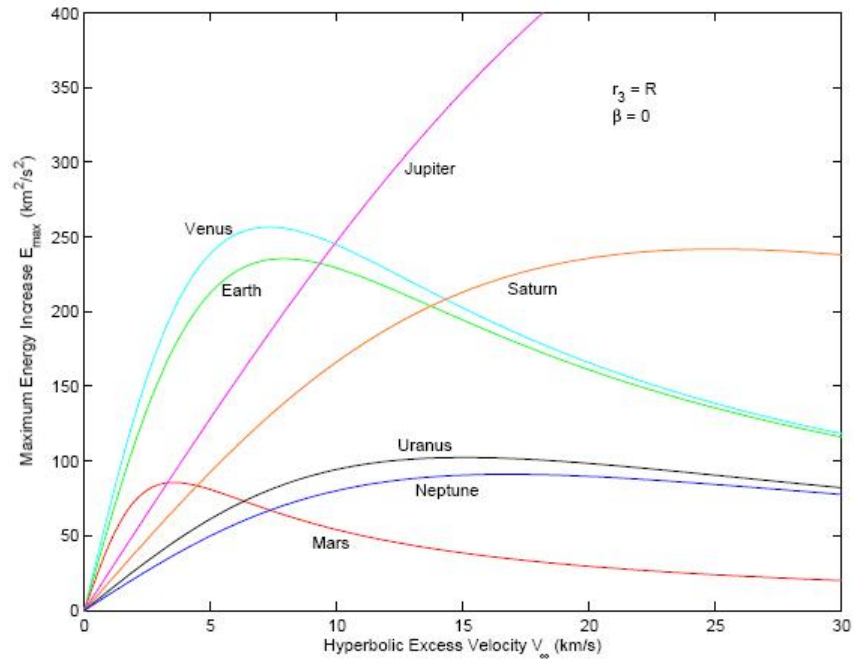


Figure 27: Maximum heliocentric energy increase for planetary swingby missions [Melman, 2007].

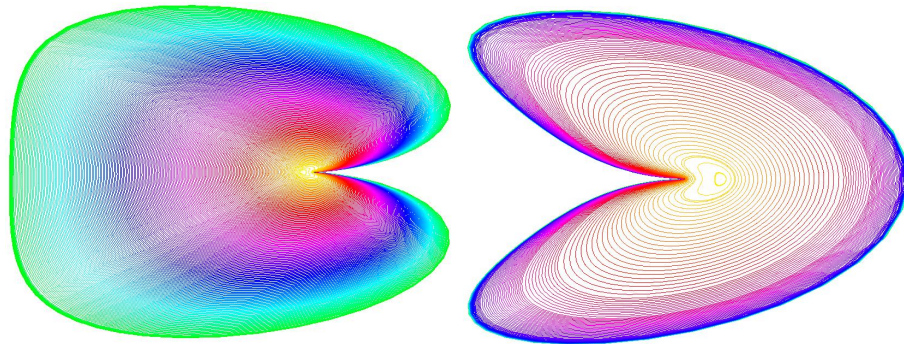


Figure 28: Example of a family of planar periodic orbits about the L_1 and L_2 libration points, generated by AUTO.

7.3 Possibilities for transfer

Plotting the manifolds emanating from the inner planet's L_2 and the outer planet's L_1 periodic orbits in one figure shows the possibilities for transfer in Figures 29 to 32. Plots are in kilometers in an inertial reference frame; both families of manifolds have been rotated according to the planet positions and seconds after J2000 ($\theta_0 = \theta_{J2000}$). The manifolds are plotted for minimal energy levels, emanating from the periodic orbits as given in Table 13.

Planet	C_{L_1} [-]	C_{L_2} [-]
Mercury	2.998	2.998
Venus	2.998	2.908
Earth	2.964	2.992
Mars	2.996	2.998
Jupiter	2.142	2.910
Saturn	2.287	2.942
Uranus	2.683	2.973
Neptune	2.824	2.970

Table 11: Maximum energy levels w.r.t. the rotating reference frame, derived from AUTO.

Planet	E_{L_1} [km^2s^{-2}]	E_{L_2} [km^2s^{-2}]	$E_{L_1(i+1)} - E_{L_2(i)}$ [km^2s^{-2}]	ΔE_{max} [km^2s^{-2}]
Mercury	-1163	-1128	492	-
Venus	-636	-591	130	250
Earth	-461	-426	129	230
Mars	-297	-286	175	80
Jupiter	-111	-64	9	400
Saturn	-55	-38	13	240
Uranus	-25	-21	5	100
Neptune	-16	-13	-	-

Table 12: Summary of standard minimum inertial energy levels for libration points and their energy gap, and possible swing-by energy increments.

Planet		x_0 [-]	\dot{y}_0 [-]	T [-]	C [-]
Earth	L_2	1.011	-0.00698	3.0828	3.00085
Mars	L_1	0.995	0.00177	3.0308	3.0002
Jupiter	L_2	1.08	-0.0806	3.2588	3.03192
Saturn	L_1	0.95	0.03792	.9806	3.0170
Saturn	L_2	1.047	-0.02488	3.1312	3.01741
Saturn	L_2	1.08	-0.1595	5.6376	2.9989
Uranus	L_1	0.979	-0.002038	3.0184	3.00492
Uranus	L_2	1.027	-0.01728	3.1134	3.00491
Neptune	L_1	0.977	-0.0167	3.0006	3.00561

Table 13: Characteristics of initial periodic orbit used for the generation of manifolds, in normalized units.

The figures show that for minimum energy levels only overlap in position exists for manifolds from Jupiter to Saturn (Figure 30) and from Uranus to Neptune (Figure 32), as indeed was indicated by the smaller gap in minimum inertial energy (Table 12). The difference in velocity and needed maneuvers to connect the manifolds will be discussed in the next chapter.

Increasing the energy level of the periodic orbit about the L_2 libration point of the Sun-Saturn system to 2.9989, shows (Figure 33) that for higher energy levels intersections become apparent and interplanetary transfer along manifolds is possible. However, this energy level or velocity needs to be obtained first,

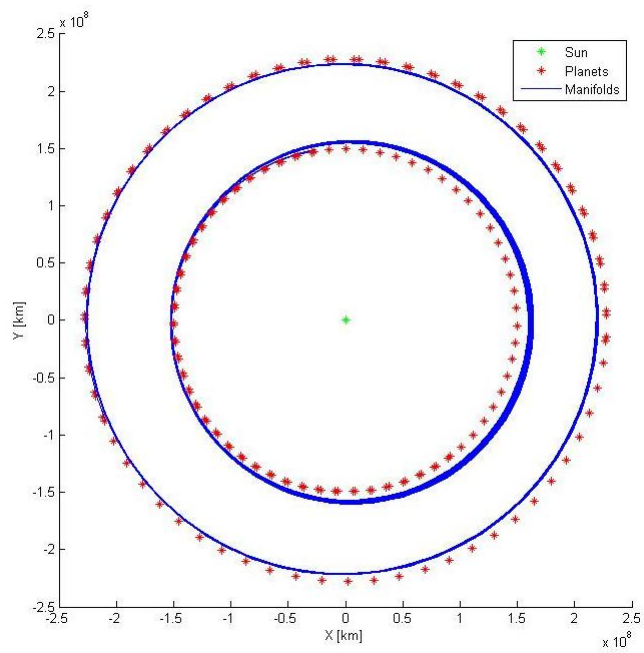


Figure 29: Manifolds from Earth's L_2 and to Mars' L_1 , for minimum energy levels.

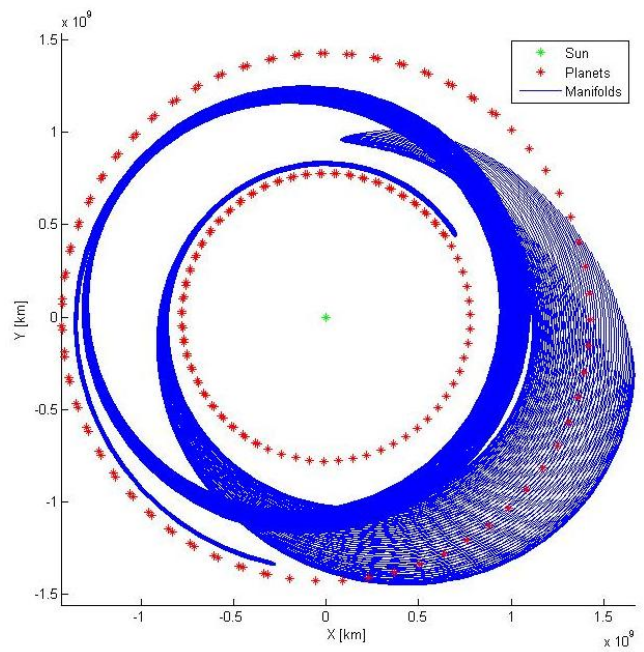


Figure 30: Manifolds from Jupiter's L_2 and to Saturn's L_1 , for minimum energy levels.

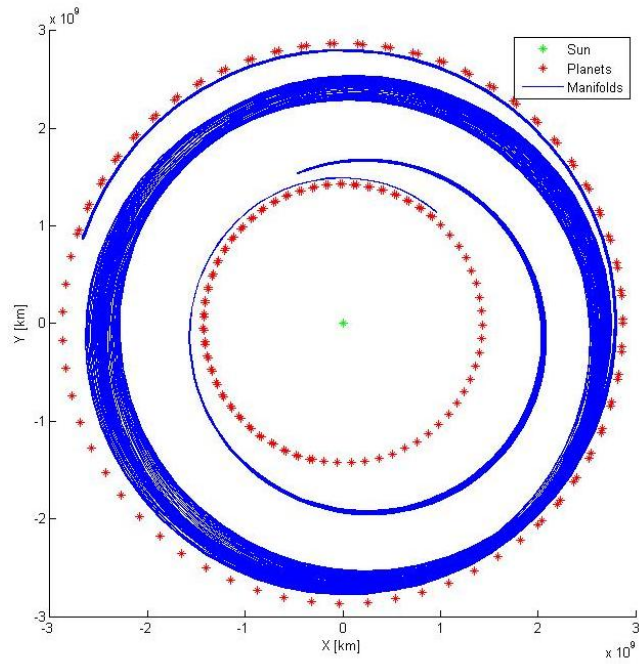


Figure 31: Manifolds from Saturn's L_2 and to Uranus's L_1 , for minimum energy levels.

increasing the total required energy for a mission. Therefore minimum energy levels are chosen for the final part of this study.

Because of the large amount of intersecting orbits for a minimum energy level, the coupled Jupiter-Saturn three-body systems will be examined in detail. In the next chapter the needed maneuver to move from Jupiter's L_2 unstable manifold onto Saturn's L_1 stable manifold is computed and analyzed for different cases.

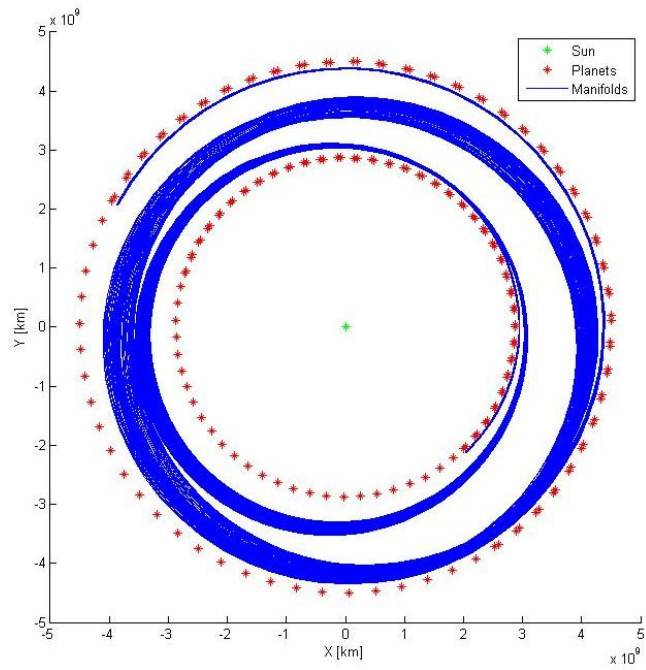


Figure 32: Manifolds from Uranus's L_2 and to Neptune's L_1 , for minimum energy levels.

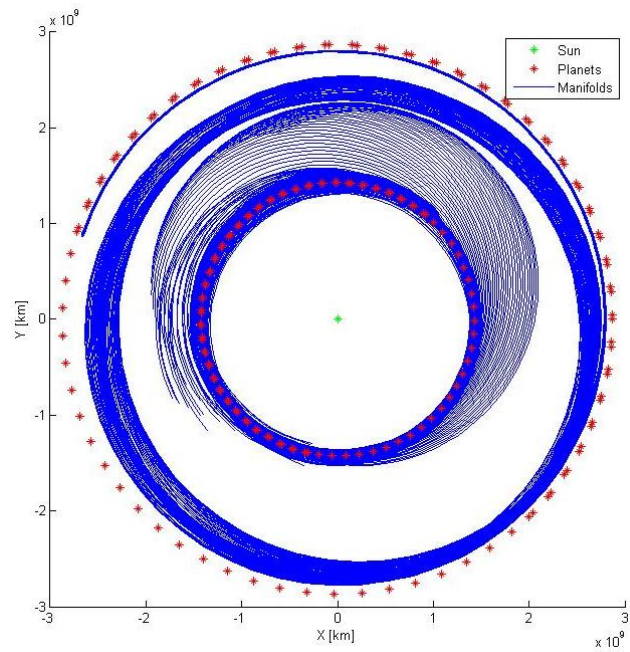


Figure 33: Manifolds from Saturn's L_2 and to Uranus's L_1 , for higher energy level.

8 Intersections in the coupled PCR3BP

Because of the planar motion of the planets involved and the extra velocity increments needed for out-of-plane maneuvers, only connections in the planar CR3BP will be examined. As shown in the previous section (Figure 30) the Jupiter and Saturn systems are most suitable for interplanetary transfer. The Poincaré section of their intersecting manifolds will be analyzed for different epochs and intersections.

8.1 Poincaré sections

Using a cross-section at $\theta = 1.5\pi = 270^\circ$ the positions of twice 100 orbits on the manifolds of Figure 30 are shown in Figure 34, with respect to an inertial reference frame and in standard units. The two three-body problems are coupled for a J2000 epoch, and the location of the chosen cross-section is shown in Figure 35. As the cut is located on the negative Y axis, the position in X direction is (approximately) zero for all points. The error in X position (Figure 34) is due to precision of data generated by Tudat, which is in the order of 10^{-10} in normalized coordinates.

Figure 36 shows the velocity in both directions for both manifolds. Here Y ranges from approximately -1.5 to -1.0 10^9 km, as is in conformity with Figure 35. Typical values of V_X are from 8 to 11 km/s for Jupiter's unstable manifold, and from 10.5 to 11.5 km/s for Saturn's stable manifold. However, no overlap exists for similar positions (i.e. equal value of Y). The same can be said about the velocity in y-direction V_Y , which ranges from -3 to -1.5 km/s for the unstable manifold and from 1 to 2 km/s for the stable manifold.

This means that there will always be a difference in velocity. The figure can be used to minimize this difference, which is the needed velocity increment to maneuver from Jupiter's unstable manifold onto Saturn's stable manifold.

In order to gain a simple increase in energy only, a velocity increment in the direction of flight is preferred, so V_x over V_y should be equal for both manifolds. As Figure 37 shows, no such point exists. This is also the fact for many other cuts (not depicted), and therefore the connections will only be optimized on the size of the velocity increments.

The minimal vectorial velocity difference ($\sqrt{\Delta V_X^2 + \Delta V_Y^2}$) is to be found for overlapping positions (i.e. equal value of Y). To find these intersecting points a curve is fit to the data (2 times 100 points) of Figures 36, the result of which is shown in Figures 38.

The fit function available in MATLAB most suitable for this problem is the *nearest neighbour interpolation* method [Mathworks, 2012], because it conserves the shape of the diagrams. Other fitting methods have been tried on various test cases, such as splitting the diagram in two parts and fitting a polynomial to it. This gave approximately the same results (minimum velocity increments), and proved not suitable for the whole collection of data because of differently shaped curves, while only increasing computational effort.

The fitted curves can be sampled again, such that for any point within the overlapping positions (i.e. Y-values, since X is zero) the total velocity difference can be calculated. In order to perform this calculation, both the V_X and V_Y curves are sampled over exactly the same Y-values.

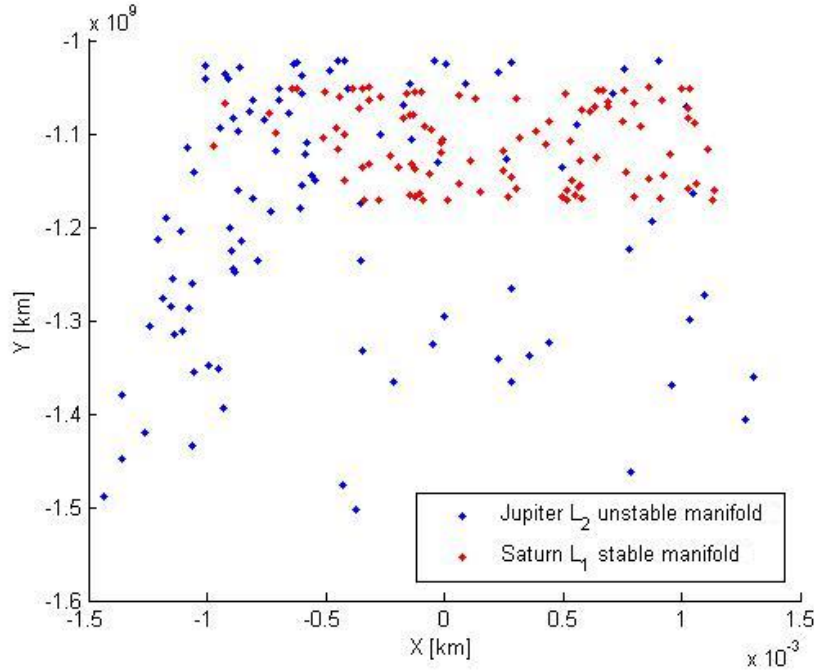


Figure 34: Cut (at 270°) of manifolds from Jupiter's L_2 and to Saturn's L_1 , for minimum energy levels.

As can be seen in both figures of Figure 38, 4 combinations of velocities exist, resulting in 4 differences in velocity in Figure 39, for every Y-value. However the resulting two curves are non-continuous, a minimum velocity difference can clearly be found.

According to the computed velocity differences, visualized in Figure 39, the minimum value for this specific epoch and cut is 2.35 km/s.

8.2 Other cuts

For the same epoch, also other cuts can be chosen. As shown in Figure 30, the manifolds intersect for angles $\theta = 1.3 - 1.6 \pi = 234 - 288^\circ$, but as the figure is symmetric, also for $\theta = 0.1 - 0.4 \pi = 378 - 432^\circ$. These angles are indicated in Figure 35.

Using the same technique as above, but rotating the figures to an new coordinate frame X, Y such that X is again zero, the minimum velocity increments for different cuts can be computed. The results are shown in Table 14 and Figure 40. The result for $\theta = 270^\circ$, obtained earlier, is also included.

It shows that the problem might be symmetric, such that when there are two places where the families of manifolds intersect, only the first needs to be examined. This was already expected when inspecting Figure 35.

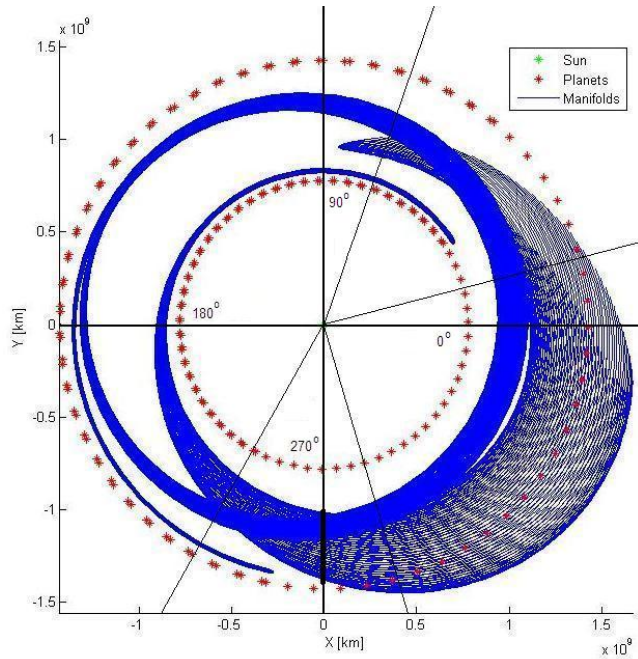


Figure 35: Location of cut (270°) and intersecting areas on manifolds from Jupiter's L_2 and to Saturn's L_1 , for minimum energy levels.

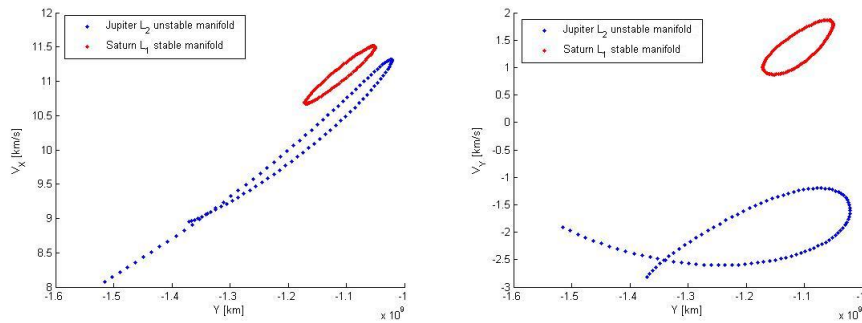


Figure 36: Velocity [km/s] in cut (at 270°) of manifolds from Jupiter's L_2 and to Saturn's L_1 .

8.3 Other epochs

Clearly, the results in terms of minimum ΔV are driven by the geometry of the two manifolds with respect to each other; in turn, this is driven by the positions of Jupiter and Saturn at the initial epoch chosen. As the synodic period of Jupiter and Saturn is 19.85887 years, the influence of this geometry can be sampled in 20 epochs. The manifolds can be converted to an inertial reference frame and visualized as before. This is shown for epochs J2000 plus 5, 10, 20 and 30 years (or the year 2005, 2010, 2020 and 2030) in Figure 41. As can be seen, the geometry of the manifolds in 2010 and 2030 is the same. This means

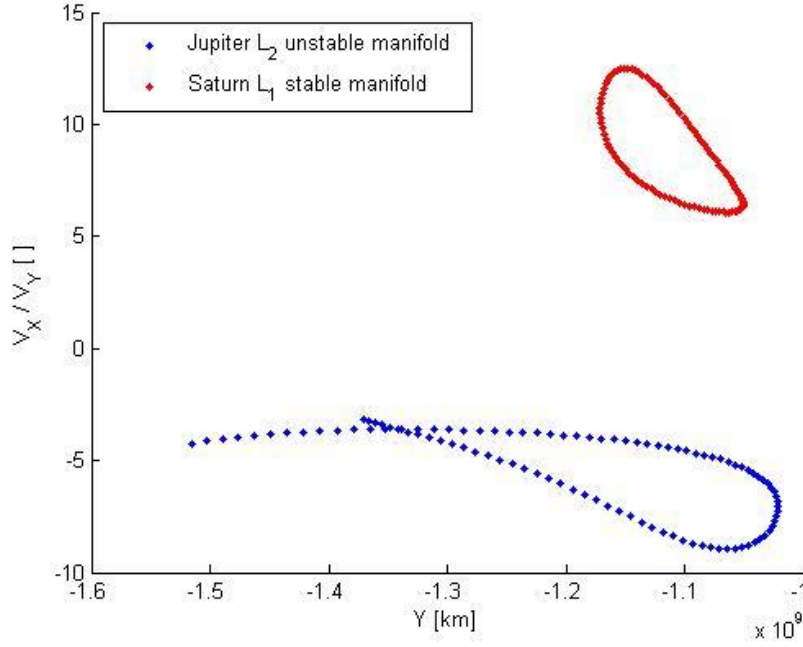


Figure 37: Velocity ratio in cut (at 270°) of manifolds from Jupiter's L_2 and to Saturn's L_1 .

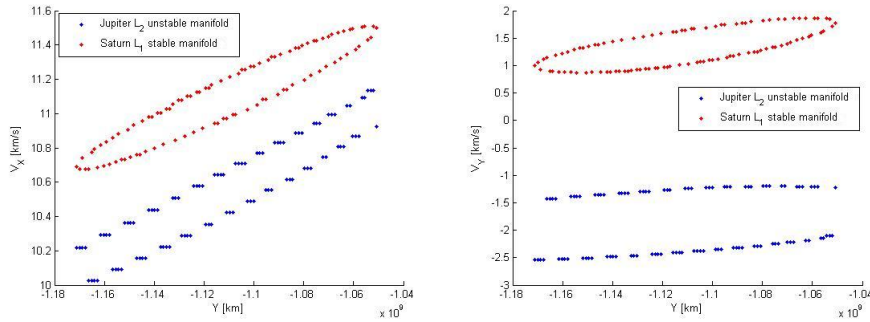


Figure 38: Interpolated velocities [km/s] in cut (at 270°) of manifolds from Jupiter's L_2 and to Saturn's L_1 .

that the relative orientation of the manifolds and their state vectors is equal, and so will be the differences in velocity.

Again in the intersecting area cuts can be chosen and the minimum velocity increment computed. The result for multiple cuts in the 2010 epoch (J2000 + 10 years) shows that the problem in general is not symmetric, as can be seen in Figure 42. To make a reasonable inventory of the options for connections, each relative geometry of manifolds is sampled by 6 different cuts, i.e. 6 cuts per epoch. The positions A to F of the cuts are given in Table 15.

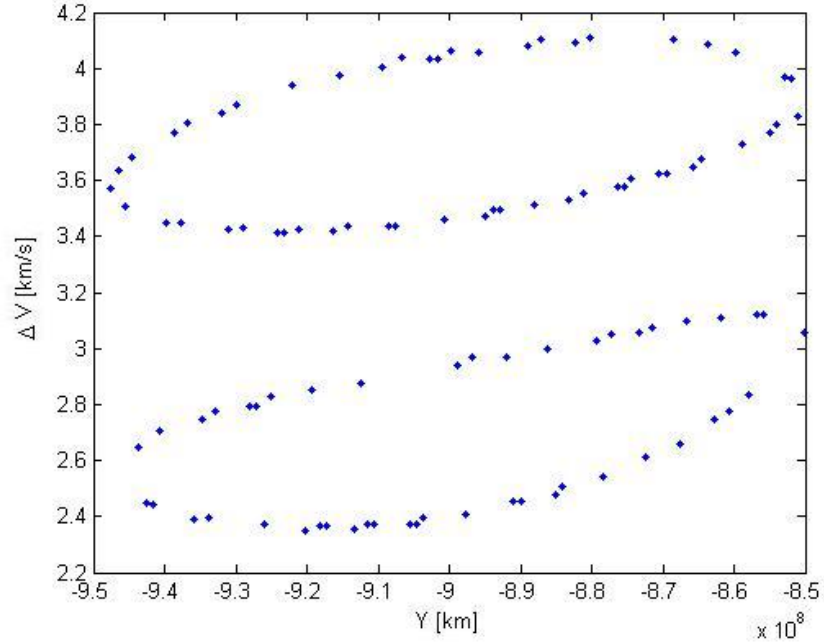


Figure 39: Velocity differences [km/s] in cut (at 270°) of manifolds from Jupiter's L_2 and to Saturn's L_1 .

Angle θ [$^\circ$]	Minimum velocity increment [km/s]
234	4.0545
252	3.2525
270	2.3483
288	1.8249
306	1.5333
324	No intersection
342	No intersection
360	No intersection
378	1.5984
396	1.9534
414	2.5252
432	No intersection

Table 14: Minimum needed velocity increments [km/s] from Jupiter's unstable manifold to Saturn's stable manifold, at different positions [$^\circ$] in the J2000 epoch.

Due to the addition of the rotation of the planets in time, the angular positions of the intersections become larger than 360° .

The minimum ΔV for each of these cuts are shown in Table 16. When no intersecting manifolds are found for a given angular position of the cut, this is indicated with NI.

	A	B	C	D	E	F
J2000	252	270	288	396	414	432
2001	270	288	306	414	432	450
2002	288	306	324	432	450	468
2003	306	342	378	432	468	504
2004	342	378	414	450	486	522
2005	378	414	450	486	522	558
2006	396	432	468	504	540	576
2007	414	450	486	522	558	594
2008	450	486	522	558	594	630
2009	495	531	567	603	639	675
2010	522	558	594	630	666	702
2011	216	252	288	324	360	396
2012	252	288	324	360	396	432
2013	288	324	360	396	432	468
2014	324	360	396	432	468	504
2015	360	396	432	468	504	540
2016	396	432	468	504	540	576
2017	414	432	450	558	576	594
2018	432	468	504	558	594	630
2019	468	504	540	576	612	648

Table 15: Angular positions [°] of cuts in intersecting Jupiter and Saturn manifolds, for different epochs [years].

	A	B	C	D	E	F
2000	3.2525	2.3483	1.8249	1.9534	2.5252	NI
2001	3.7913	2.5864	1.9754	1.8080	2.3061	3.2061
2002	4.1952	2.8149	2.0732	1.6256	2.0435	2.7955
2003	4.2969	2.1708	1.3035	1.1949	1.7549	NI
2004	3.1963	1.6445	1.0029	0.9329	1.4485	NI
2005	2.1877	1.1991	0.8100	0.8652	1.5102	NI
2006	2.1143	1.0847	0.7160	0.6654	1.1068	NI
2007	2.1581	0.9434	0.5844	0.5073	0.7671	NI
2008	1.2554	0.5834	0.3688	0.3755	0.7469	NI
2009	0.6416	0.5226	0.2486	0.3136	1.1357	NI
2010	0.5257	0.3883	0.4335	0.2026	0.9261	NI
2011	0.3411	0.2370	0.5309	0.3973	NI	NI
2012	0.9858	0.4304	0.3735	0.2174	0.5428	0.5205
2013	1.6523	0.8792	0.5173	0.3103	0.3936	0.5875
2014	2.0945	1.1817	0.6201	0.4984	0.5985	0.9506
2015	2.5711	1.3559	0.7656	0.6665	0.8707	1.5368
2016	2.5316	1.3933	0.8633	0.8539	1.3049	2.2673
2017	3.3206	2.3562	1.7863	1.3890	1.7882	2.3501
2018	3.6057	2.1555	1.3434	1.3348	1.8261	3.2342
2019	3.6010	NI	NI	NI	1.7876	3.0459

Table 16: Minimal velocity differences [km/s] in intersecting Jupiter and Saturn manifolds, for different positions of the intersection and epochs [years].

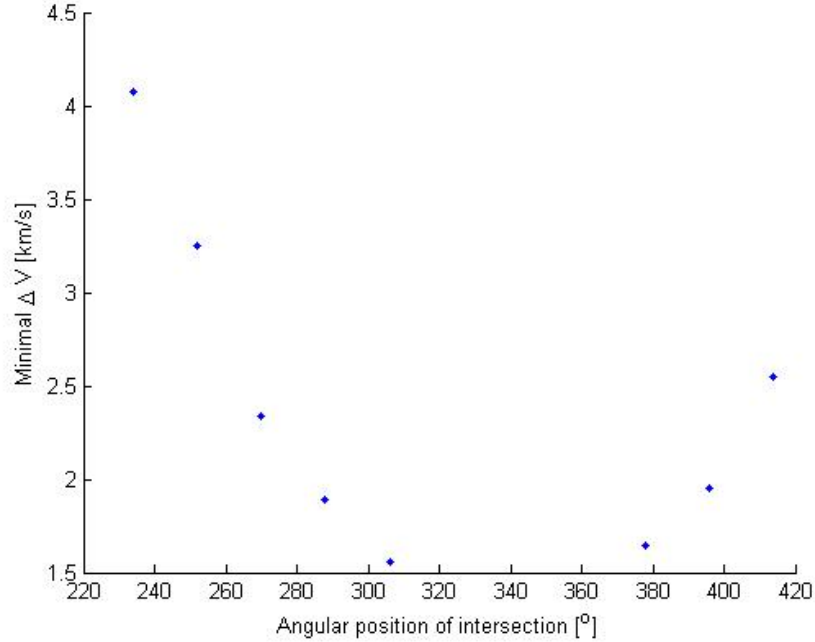


Figure 40: Minimum needed velocity increments [km/s] from Jupiter’s unstable manifold to Saturn’s stable manifold, at different positions [°] in the J2000 epoch.

8.4 Analysis

Although gridded in a coarse way (20 epochs, 6 cuts), Table 16 provides the most attractive combination of manifolds to transfer from Jupiter to Saturn, at a minimum ΔV . Because interpreting a table can be rather cumbersome, the minimal values for every intersection are visualized for each epoch in Figure 43 and in a contour plot in Figure 44. The contour plot relates to the 3-dimensional graph (epoch, intersection, ΔV) of which Figure 43 is formed by the vertical cross-sections for the 20 different epochs.

The intersections chosen in the middle give the most optimal results, this is presumably due to the orientation of the manifolds with respect to each other. The orbits forming the manifolds are aligned at this point, as well as the velocity vectors, decreasing the need for a maneuver. As Figure 43 shows, the choice of the position of the intersection is most important for the first and last years in this range of epochs, while the 2009-2012 epochs show straighter curves.

Furthermore there are indications, such as Figure 44, that the behaviour is cyclic. Which makes sense, knowing that for every epoch only the relative positions of the planets change. So after each synodic period of approximately 20 years the pattern will repeat and there will be another, similar, minimum around 2030. This can also be seen from the total minimal velocity increments per epoch, in Figure 45.

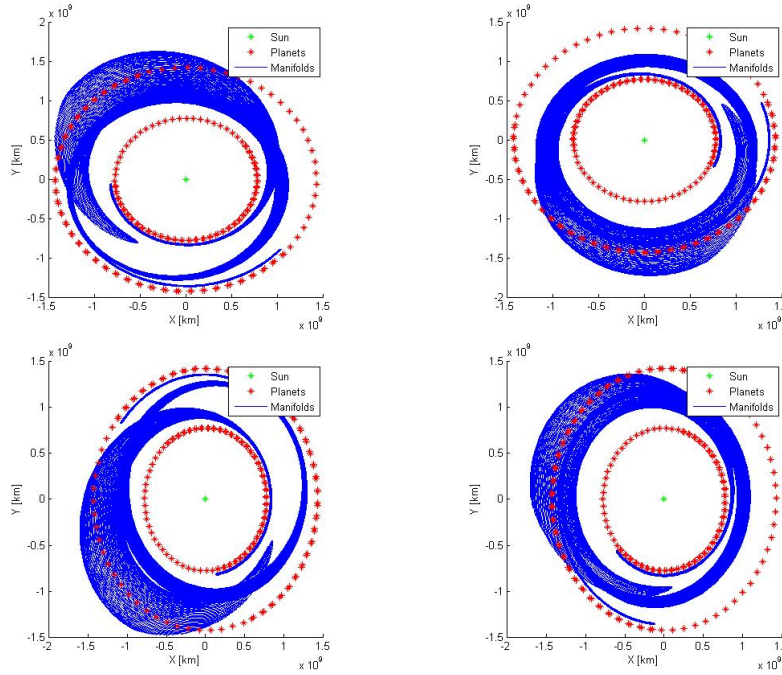


Figure 41: Manifolds from Jupiter's L_2 and to Saturn's L_1 , with respect to the inertial reference frame in the year 2005, 2010, 2020 and 2030.

Table 16 suggests that the optimal transfer can be found for the year 2010 and an angle of 630° . To more accurately identify the minimal maneuver, the intersections around 630° for the 2010 epoch are examined more closely. Figure 46 shows that the minimal velocity increment is about 200 m/s, for $\theta = 632^\circ$. This is an improvement of approximately 3 m/s with respect to the previous best result. As the Poincaré cuts of Figure 47 show, matching values of V_Y can be found, and there is only a difference in velocity in X-direction, which proves the similar orientation of the state vectors.

Based on the results of this chapter, the minimum needed velocity increments to maneuver from one planet's unstable manifold to the next planet's stable manifold are found when the manifolds have the most overlap and they have the same orientation. Rotating the obtained manifolds according to the planet positions for different epochs, already a quick qualitative analysis can be made to choose time and position of intersection.

The minimal required velocity increment for all epochs and intersections calculated is 200 m/s. This value is used in the design of the mission and compared to other means of interplanetary transfer in the next chapter.

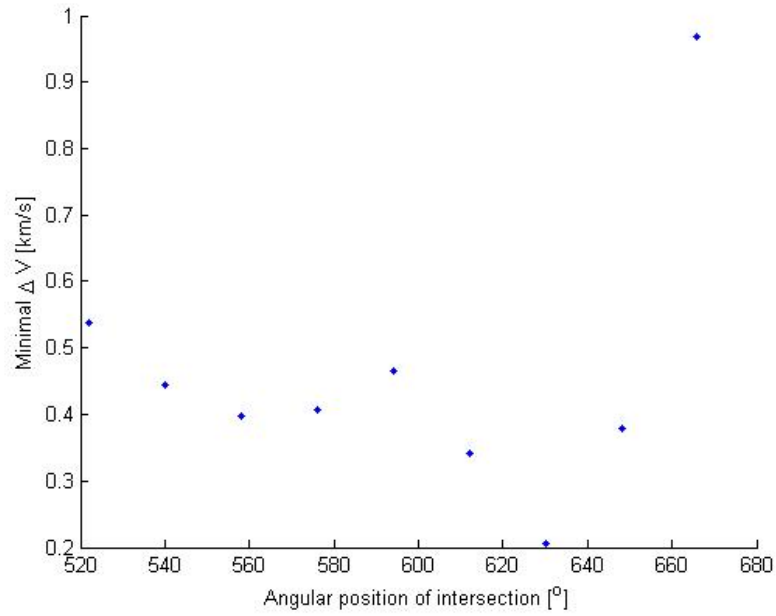


Figure 42: Minimum needed velocity increments [km/s] from Jupiter's unstable manifold to Saturn's stable manifold, at different positions [°] in the 2010 epoch.

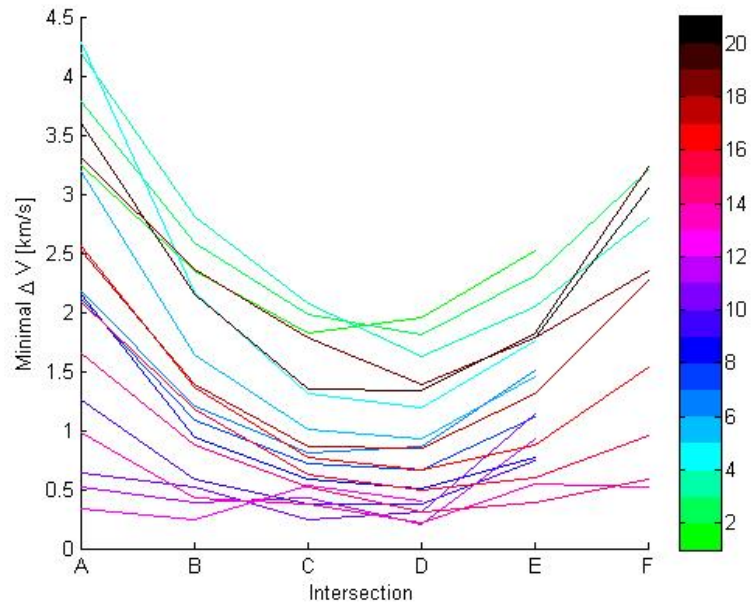


Figure 43: Minimum needed velocity increments [km/s] from Jupiter's unstable manifold to Saturn's stable manifold, for different intersections and epochs [years].

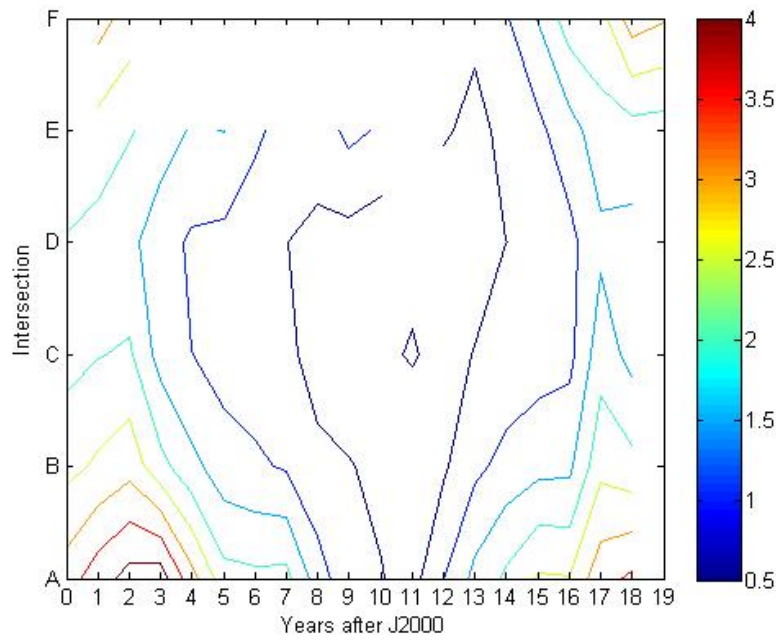


Figure 44: Minimal velocity differences [km/s] in intersecting Jupiter and Saturn manifolds, for different positions of the intersection and epochs [years].

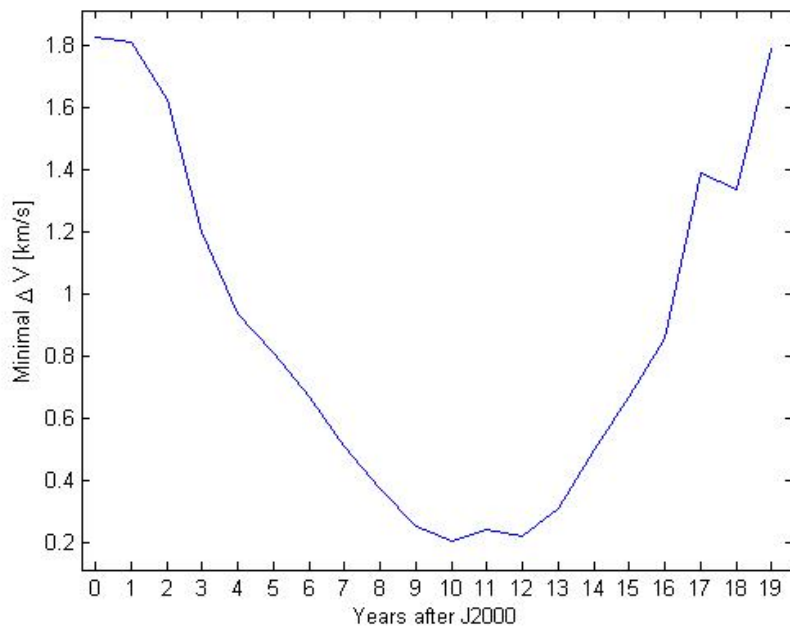


Figure 45: Minimum needed velocity increments [km/s] from Jupiter's unstable manifold to Saturn's stable manifold, for different epochs [years].

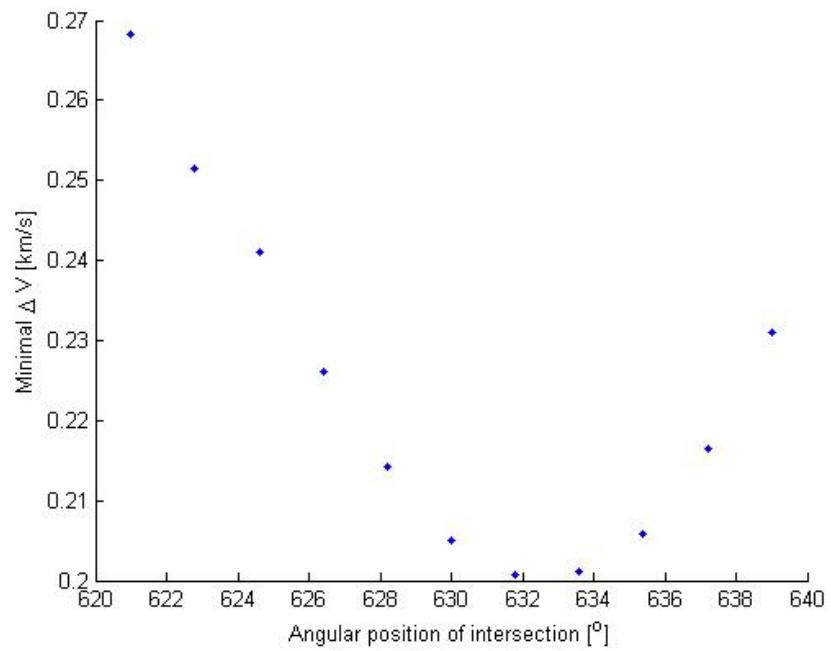


Figure 46: Minimum needed velocity increments [km/s] from Jupiter's unstable manifold to Saturn's stable manifold, for different positions [°] in the 2010 epoch.

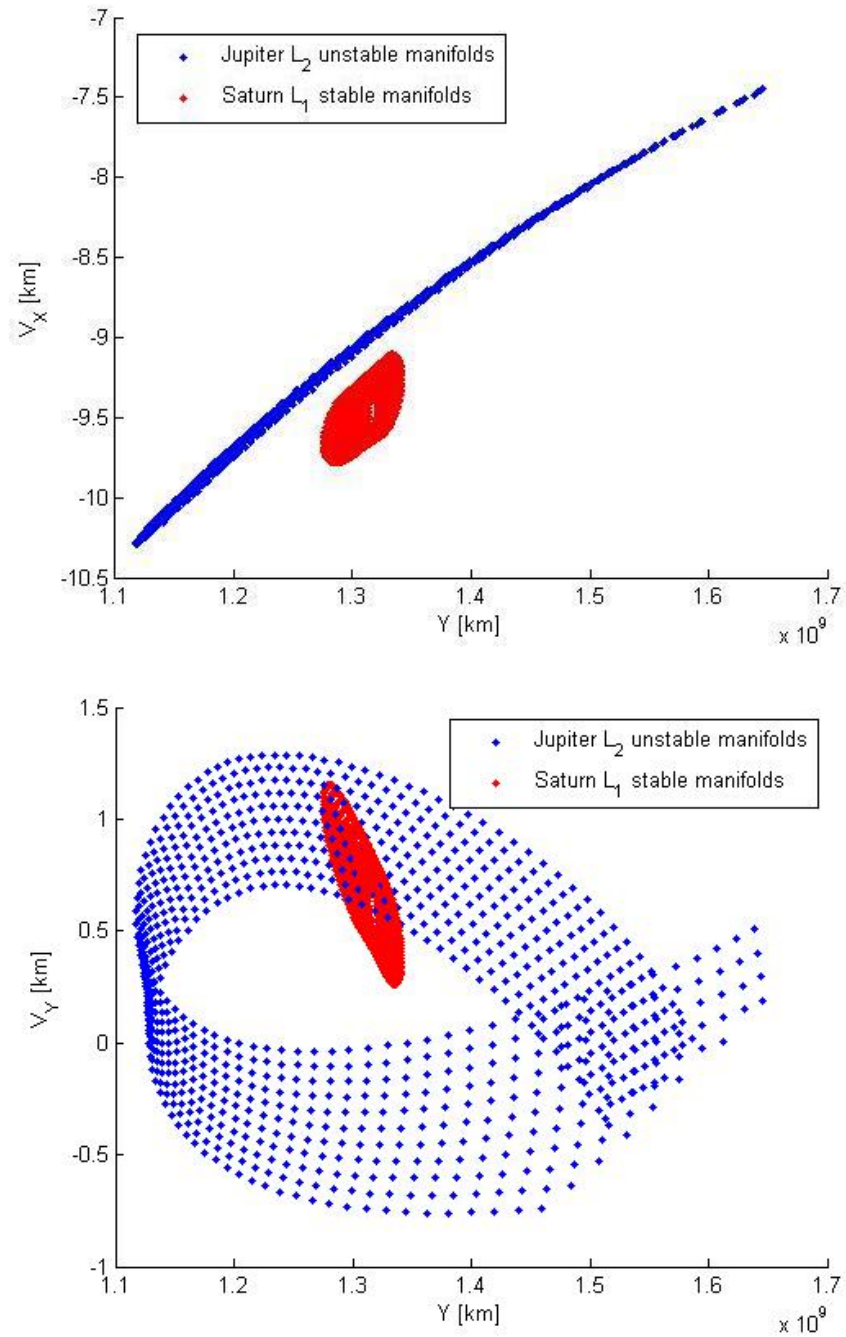


Figure 47: Velocities [km/s] in cut of manifolds from Jupiter's L_2 and to Saturn's L_1 , for different angular positions ($620 - 640^\circ$) in the 2010 epoch.

9 Discussion of results

The main result of the previous chapter is a minimum velocity increment to change from an unstable manifold emanating from Jupiter's L_2 planar periodic orbit onto Saturn's L_1 stable manifold, for minimum energy conditions. Of course, this transfer cannot exist by itself: it is part of a transfer from a parking orbit about Jupiter to a parking orbit about Saturn. The total transfer must be compared to a classical Hohmann transfer. Based on this, the feasibility of interplanetary transfer using manifolds is discussed.

9.1 Comparison to Hohmann transfer

As explained in Chapter 2, the minimum velocity increments needed in the classic 2-body approach are based on a Hohmann transfer. The total velocity increments needed for such a transfer can be used for comparison.

The assumed radius of both the circular parking orbit about Jupiter and about Saturn, is 1.1 planetary radii. Used quantities, such as the circular velocity in these orbits V_c , are stated in Table 17.

Planet	μ_P [$10^6 \text{ km}^3/\text{s}^2$]	R_p [km]	R_{park} [km]	$V_c(R_{park})$ [km/s]
Jupiter	126.686	71492	78641	40.12
Saturn	37.931	60268	66295	23.92

Table 17: Values needed to compute velocity increments in Hohmann transfer between Jupiter and Saturn [NASA, 2010].

Assuming a pericenter at the distance of Jupiter (5.2034 AU) and an apocenter at the distance of Saturn (9.5371 AU), the interplanetary transfer is one half of an ellipse about the Sun. It has a semi-major axis of 7.37025 AU or 1102574660 km and an eccentricity of 0.294, which yields a pericentric and apocentric heliocentric velocity of respectively 14.85 and 8.10 km/s.

Subtracting the orbital velocity of Jupiter (13.06 km/s [Wakker, 2007b]), the velocity V_∞ relative to this planet to be obtained at departure is 1.80 km/s. Doing the same for Saturn's orbital velocity of 9.64 km/s, the velocity V_∞ relative to Saturn at arrival should be 1.54 km/s. Furthermore at least the velocity V_{esc} is needed to escape Jupiter's surroundings:

$$V_{esc} = \sqrt{\frac{2\mu}{r}} \quad (73)$$

$$V = \sqrt{V_{esc}^2 + V_\infty^2}$$

At a distance r of the parking orbit and using the values for V_∞ just found, the velocities V are respectively 56.76 and 33.86 km/s. This means an acceleration of 16.65 km/s is needed at departure and a deceleration of 9.94 km/s is needed at arrival, resulting in a total required ΔV of 26.59 km/s for the Hohmann transfer. According to Equation 9 this transfer would take 10 years.

For the transfers by means of DST as presented in this thesis, still a transfer from the parking orbit to the libration points and vice-versa is needed. For the computation of these maneuvers, some values are given in Table 18. Note

that the libration points are not within the sphere of influence of Jupiter nor Saturn, which measure respectively a maximum of 50.5 and 57.7 10^6 km [Wakker, 2007a]. This means that the Hohmann transfer is only an approximation for the needed velocity increment to get from the parking orbit to a height of the libration points.

As shown in Figure 48, the Hohmann orbit has its pericenter at the parking orbit and its apocenter at a height of the periodic orbit about L_2 , such that the pericenter velocity is 56.72 km/s. The difference between the velocity in the parking orbit and the pericenter velocity is 16.58 km/s. The ellipse is defined with respect to Jupiter, while the libration points are fixed with respect to the Sun. Adding the velocity of Jupiter to the apocenter velocity (0.08 km/s), the velocity at L_2 is 13.14 km/s with respect to the Sun. Given the periodic orbit from Table 13, the minimal velocity to be obtained is -1.05241 km/s plus the circular velocity of L_2 with respect to the Sun, or 11.57 km/s in total. The difference between the apocenter velocity and that of the periodic orbit (both with respect to the Sun) is the velocity increment to get from the Hohmann orbit onto the periodic orbit about L_2 and is 1.57 km/s. Together with the first velocity increment of 16.58 km/s to maneuver from the parking orbit to the Hohmann-orbit, this results in a ΔV of 18.15 km/s.

Planet	$R_{L_i}^{planet}$ [km]	$R_{L_i}^{Sun}$ [km]	V_{c,L_i}^{Sun} [km/s]
Jupiter	54297488	832715048	12.62
Saturn	64153072	1362572340	9.87

Table 18: Values needed to compute velocity increments to transfer from and to the libration points.

The same can be done to get from the periodic orbit about Saturn's L_2 with a velocity of 0.37 km/s with respect to Saturn or 9.50 km/s with respect to the Sun, to a Hohmann orbit (Figure 48). This elliptical orbit has its apocenter at a distance of the libration point, which yields a velocity of 0.03 km/s. Adding the circular velocity of Jupiter in its orbit about the Sun, the satellite needs to be accelerated to 9.67 km/s, resulting in the first velocity increment of 0.17 km/s. Next the pericenter velocity of 33.81 km/s needs to be lowered to the velocity of the parking orbit (Table 17), resulting in a velocity increment of 9.89 km/s. Together the two maneuvers result in a ΔV of 10.07 km/s.

So first a transfer from the parking orbit of 1.1 Jupiter radii about this planet to a specified periodic orbit about its L_2 libration point is used. This results in a total ΔV of 18.15 km/s. Then after the manifolds form the connection between the two libration points, a transfer from near Saturn's L_1 libration point to a parking orbit at 1.1 Saturn radii needs two more velocity increments, with a total of 10.07 km/s. Including the 0.2 km/s needed to change from Jupiter's unstable manifold onto Saturn's stable manifold, this results in a total of maneuvers of 28.42 km/s, which is more than the budget needed for a classical Hohmann transfer.

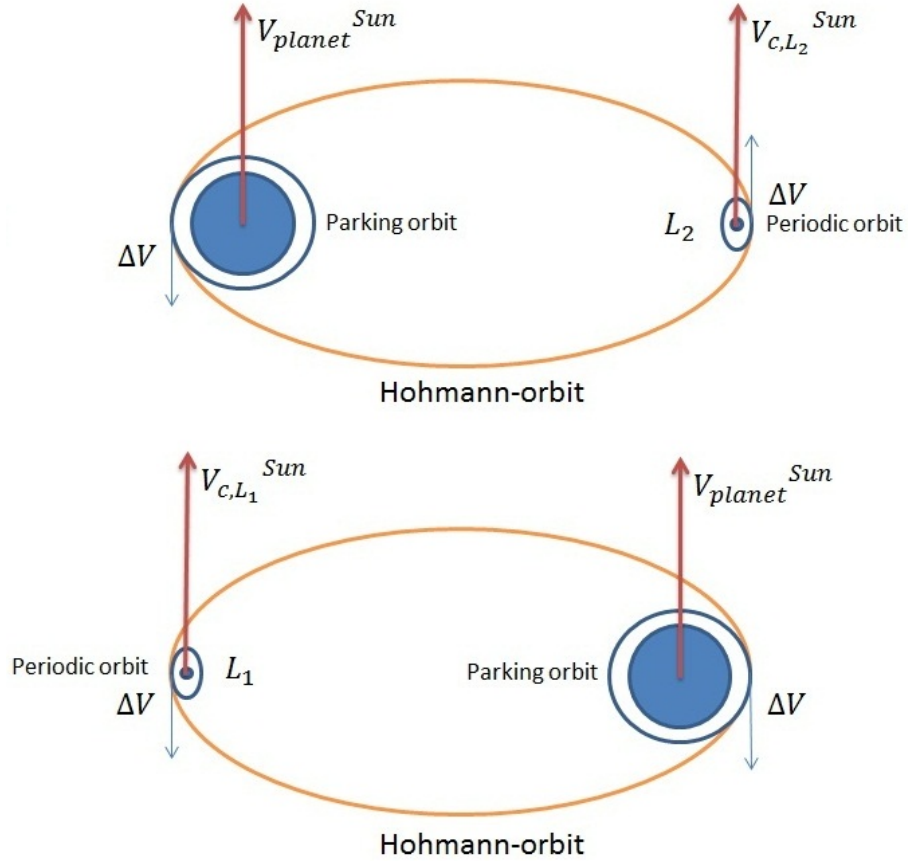


Figure 48: Hohmann orbits in the total transfer using DST, in the Jupiter (top) and Saturn (bottom) systems.

9.2 Feasibility of the mission

The higher energy requirement does not mean the mission from Jupiter to Saturn using DST is unfeasible. Other methods to get to and from the libration points can be used, such as gravity assists about moons or using the planet-moon manifolds. Orbits using the latter technique have been constructed in various studies concerning the coupled Earth-Moon and Sun-Earth three-body systems, such as [Howell, 2006] and [Moore, 2009].

A mission visiting both Jupiter and Saturn using only gravity assists is due to geometric constraints and the rare launch window almost impossible [Lali, 2009]. Using manifolds would be a great opportunity to observe both planets, as Figure 17 shows that only minor errors in energy (or initial velocity) cause the satellite to orbit the secondary body instead of the libration point. [Wang, 2009], [Doedel, 2010] and [Calleja, 2011] show how manifolds are to be used in a low-energy mission orbiting Earth, moon and their libration points, which can easily be extended to the Sun-planet cases of this report.

The required accuracy is a drawback of transfer by manifolds and may be an important constraint for missions to and between the outer planets. Therefore low thrust might be more suitable, than the instantaneous maneuvers used in this study.

Another drawback is the time required for transfer: in the Jupiter-Saturn case that has been optimized it would result in approximately 20 years, which however can simply be lowered when larger deviations from the periodical orbit are used, as is shown in Figure 24.

So in the current state of development of the use of DST for space flight, interplanetary transfer using manifolds would not be feasible. The low velocity increments -in the order of 100's of m/s- required for maneuvering from one planet's unstable manifold onto the next planet's stable manifold, however make it an option worth investigating as a means of transfer in future missions, especially to and between the outer planets and their libration points.

10 Conclusions and Recommendations

In this study manifolds in the coupled planar circular restricted three-body problem as means of interplanetary transfer are examined.

The motion of a body in space is defined by the gravitational attraction of all other bodies. In a system of three bodies some assumptions can be made, leading to the circular restricted three body problem (CR3BP). This results in two major bodies moving in circular coplanar orbits about each other, while the smaller body (with negligible mass) is not confined to this type of motion. The plane of the two major bodies defines a rotating reference frame. In this reference frame and after normalizing mass, distance and time, the resulting three second-order differential equations are the equations of motion of the CR3BP. The problem is now only dependent on the mass parameter, which is based on the mass ratio of the two major bodies.

The Sun-planet-satellite three-body systems fulfill the restrictions of the CR3BP. The equations of motion can be translated to 6 first-order differential equations, with the Jacobi energy integral as a conservative quantity.

Analyzing the energy surfaces and the equations of motion, equilibrium points are found, called libration points. Linearizing the equations, the region around these points shows 4 types of motion: periodic, transit, non-transit and asymptotic. The asymptotic orbits towards the equilibrium region (or invariant manifold) are called stable manifolds, while the ones departing it are called unstable manifolds. They form tubes in space, being the separation between transit and non-transit orbits. So a path within these tubes will always lead to or from the periodic orbit. The 4-body problem can be approximated by coupling two three-body models with only one of the major bodies not in common.

The positions of the libration points are computed with Tudat for the Earth-Moon system and show no discrepancies when comparing to literature. Also the positions of the collinear libration points of all Sun-planet systems of the solar system, are accurate when compared to values from AUTO.

The periodic orbits can be found in the non-linearized case by means of differential correction, which is implemented in Tudat. This technique is very sensitive to changes in energy and initial conditions, such that the periodic orbits may be centered about the planet and not about the libration point. Therefore a check of the geometry of the resulting periodic orbit is always required. In this way, via a simple grid search and differential correction, the periodic orbits for a given energy level can be found. The found periodic orbits are compared on initial state, energy level and period with data from literature and the implementation shows to be valid.

Both the RK4 and RK78 integrators have been proven to be accurate by means of Tudat's obligatory unit tests and when integrating periodic orbits and manifolds. In most cases the RK4 integrator has been used because of the required expansion of the integrator: integration until a stopping condition rather than a fixed end time, and adjustment of the step size near violation of this condition, to find an accurate result.

The starting points of the manifolds can be found by deviating at a number

of points on the periodic orbit in the direction of an eigenvector of the monodromy matrix, which is the state transition matrix (STM) of the periodic orbit after one period, based on linearized equations of motion. The local eigenvectors can be computed along the periodic orbit by using the STM again.

The size of the deviation should be as large as possible, to get from the equilibrium region in the least amount of time, without giving in on accuracy. The accuracy of the manifolds can easily be evaluated by computing the variation of the constant Jacobi energy constant along a manifold.

From each periodic orbit a collection of 100 orbits is generated, forming a manifold. The unstable manifold is integrated forward from the L_2 libration point, while the stable manifold is integrated backwards from the L_1 libration point. Interplanetary connections can be found at the intersection of these two families of manifolds, for two different three-body systems.

To couple the systems, the state, time and energy have to be converted back to standard units and an inertial reference frame. The first conversion is shown to be nothing but a multiplication by the normalizing factor. The minimal energy level corresponds to that of the libration point, while the maximum energy level is derived from the outermost periodic orbit as generated by AUTO. The total energy in the inertial reference frame is not a constant, but analysis of the gaps in minimum energy between two consecutive planets, indicates that only four coupled systems have possibilities for transfer along manifolds. From the Earth-Mars, Jupiter-Saturn, Saturn-Uranus and Uranus-Neptune coupled three-body systems, only Jupiter-Saturn and Uranus-Neptune show overlap in manifolds for minimum energy conditions. These two connections indeed correspond to the smallest energy gaps. As expected, increasing the energy of Saturn's L_2 periodic orbit shows more possibilities for transfer between Saturn and Uranus.

The transfer between Jupiter and Saturn is chosen for optimization. Within the area of intersection of the manifolds different cuts can be made, resulting in 2 times 100 state vectors per cut. The introduction of a new reference frame allows that the X-component is always zero and the vector difference in velocity V is evaluated for the same Y-component. Because the 100 points in the cut will rarely have the same Y-position, the smooth Y, V_X and Y, V_Y functions are interpolated and resampled. In this way for every cut the minimum velocity difference, equal to the velocity increment of the maneuver, is found.

The geometry of the coupled system changes in time, so the synodic period of almost 20 years is sampled, and for 20 epochs and 6 cuts per epoch the minimum velocity increments are computed.

Analysis of the minima per epoch, shows they are not symmetric over the overlapping area. Over all epochs it however is clear that the cut should be chosen in the middle. This might be due to the suitable orientation of the manifolds relative to each other.

For the initial epoch 2010 (J2000 plus 10 years) a minimum is found and the behaviour of the minima over the years is shown to be cyclic, such that another minimum should be found when starting the manifolds in 2030.

Referring again to the relative orientation of the manifolds for this epoch, the alignment of manifolds seems to be the most important factor in finding a minimum-energy transfer. This means the optimal time and place of a maneuver can already be deduced from the geometry or plots of the manifolds of

coupled systems for different epochs. These plots can therefore be an important tool in the design of a mission with transfer by manifolds.

The overall minimal velocity increment is about 200 m/s, which makes manifolds by itself a promising way of transfer.

Using manifolds in the transfer from a parking orbit about Jupiter to a parking orbit about Saturn, leads to a total required velocity increment of 28.42 km/s, while a classical Hohmann transfer requires 26.59 km/s. This means that with these type of flights from and to the libration points, and the increased transfer time, transfer by means of manifolds is not to be preferred.

Other means of getting to and from the libration points or missions only visiting the libration points and their manifolds should be considered, as well as low-thrust propulsion. The obtained trajectory can then be refined in the full 4-body model, to confirm validity of the coupled three-body models.

The behaviour of the minimal velocity increments over time, can be examined more into depth when considering the epochs after 2020 and other coupled three-body systems.

As shown, more connections become apparent for higher energy levels. This may decrease the needed velocity increment further for the studied combination of Sun-planet systems and yield more possibilities for transfer for all Sun-planet systems. So simulation of the manifolds for high energy levels may really show the Interplanetary Superhighway, through which a spacecraft travels the solar system without propulsion...

References

- AUTO, *AUTO: Software for continuation and bifurcation problems in ordinary differential equations*, <http://indy.cs.concordia.ca/auto/>, last accessed 14/01/2012, 2010.
- Broucke, R., *Periodic Orbits in the Restricted Three-Body Problem with Earth-Moon Masses*, NASA-JPL Technical Report 32-1168, 1968.
- Broucke, R., Boggs, D., *Periodic orbits in the planar general three-body problem*, *Celestial Mechanics and Dynamical Astronomy*, vol. 11, pp. 13-38, 1975.
- Burden, R.L., Faires, J.D. *Numerical Analysis*, 7th Edition, Books/Cole, 2001.
- Calleja, R.C., Doedel, E.J., Humphries, A.R., Oldeman, B.E., *Computing Invariant Manifolds and Connecting Orbits in the Restricted Three Body Problem*, ArXiv e-prints, 1111.0032, 2011.
- Deurloo, R.A., *A Search for Low-Energy Capture Orbits around Jupiter Using the Influence of Galilean Moons*, MSc. Thesis, Faculty of Aerospace Engineering, Delft University of Technology, the Netherlands, 2003.
- Doedel, E.J., Oldeman, B.E., *AUTO-07P: Continuation and bifurcation software for ordinary differential equations*, Concordia University, 2009.
- Doedel, E.J., *Numerical analysis of nonlinear equations*, Lecture Notes, Concordia University, 2010.
- Doxygen, *Generate documentation from source code*, www.doxygen.org, last accessed 28/04/2011, 2011.
- Elvik, S., *Optimization of a low-energy transfer to Mars using Dynamical Systems Theory and low-thrust propulsion*, MSc. Thesis, Faculty of Aerospace Engineering, Delft University of Technology, the Netherlands, 2004.
- Fehlberg, E., *Some Old and New Runge-Kutta Formulas, with Stepsize Control and Their Error Coefficients*, *Computing*, vol. 34, pp. 265-270, 1985.
- Gomez, G., Koon, W.S., Lo, M.W., Marsden, J.E., Masdemont, J., Ross, S.D., *Invariant Manifolds, the Spatial Three-Body Problem and Space Mission Design*, AAS/AIAA Astrodynamics Specialists Conference, 2001.
- Gomez, G., Koon, W.S., Lo, M.W., Marsden, J.E., Masdemont, J., Ross, S.D., *Connecting orbits and invariant manifolds in the spatial restricted three-body problem*, *Nonlinearity*, vol. 17, pp. 1571-1606, 2004.
- Guzman, J.J., Cooley, D.S., Howell, K.C., Folta, D.C., *Trajectory design strategies that incorporate invariant manifolds and swingby*, AAS/GSFC International Symposium on Space Flight Dynamics, pp. 98-349, 1998.

- Herman, J., *TBD*, MSc. Thesis, Faculty of Aerospace Engineering, Delft University of Technology, the Netherlands, 2012.
- Howell, K.C., Pernicka, H.J., *Three-dimensional periodic Halo orbits*, Celestial Mechanics and Dynamical Astronomy, vol. 32, no. 1, pp. 53-71, 1984.
- Howell, K.C., Pernicka, H.J., *Numerical Determination of Lissajous Trajectories in the Restricted Three-body Problem*, Celestial Mechanics and Dynamical Astronomy, vol. 41, no. 1-4, pp. 107-124, 1988.
- Howell, K.C., Kakoi, M., *Transfers between the Earth-Moon and Sun-Earth systems using manifolds and transit orbits*, Acta Astronautica, vol. 59, no. 1-5, pp. 367-380, 2006.
- James, J.D., *Celestial Mechanics Notes Set 5: Symmetric Periodic Orbits of the Circular Restricted Three Body Problem and their Stable and Unstable Manifolds*, 2006.
- Koon, W.S., Lo, M.W., Marsden, J.E., Ross, S.D., *Heteroclinic connections between periodic orbits and resonance transitions in celestial mechanics*, CHAOS, vol. 10, no. 2, pp. 427-468, 2000.
- Koon, W.S., Lo, M.W., Marsden, J.E., Ross, S.D., *Dynamical Systems, the Three-Body Problem and Space Mission Design*, CalTech, 2006.
- Kumar, K., *Weak Capture and the Weak Stability Boundary*, MSc. Thesis, Faculty of Aerospace Engineering, Delft University of Technology, the Netherlands, 2008.
- Lali, M., *Analysis and Design of a Human Spaceflight to Mars, Europa, and Titan*, AIP Conf. Proc. 1208, pp. 557-565, 2009.
- Marsden, J., *Invariant Manifolds and Coherent Structures*, Control and Dynamical Systems, CalTech, 2006.
- Mathworks, *Interpolants: Interpolation and Smoothing (Curve Fitting Toolbox TM)*, http://www.mathworks.nl/help/toolbox/curvefit/bq_5ka_1.html, last accessed 20/01/2012.
- McMillan, S., *Computational Physics: Integrators* <http://einstein.drexel.edu/courses/Comp.Phys/Integrators/rk4.html>, last accessed 24/04/2011.
- Melman, J., *Trajectory Optimization for a Mission to Neptune and Triton*, Thesis Report, Delft University of Technology, the Netherlands, 2007.
- Melman, J., *Tudat Commandments and Guidelines*, Tudat Working Group, Delft University of Technology, the Netherlands, 2011.

- Montenbruck, O., Gill, E. *Satellite Orbits: Models, Methods and Applications*, Springer, 2005.
- Moore, A., *Two Approaches Utilizing Invariant Manifolds To Design Trajectories For DMOC Optimization*, Geometric Mechanics Project Archives, CalTech, 2009.
- NASA, *Interplanetary Superhighway Makes Space Travel Simpler*
http://www.jpl.nasa.gov/releases/2002/release_2002_147.html,
 last accessed 27/04/2011, 2002.
- NASA, *Planetary Fact Sheets*, <http://nssdc.gsfc.nasa.gov/planetary/factsheet>,
 last accessed 14/01/2012, 2010.
- Oldeman, B., *Computing and Continuing Invariant Manifolds and Connecting Orbits in the Restricted Three Body Problem*, presentation, Concordia University, 2011.
- Standish, E.M., *Keplerian Elements for Approximate Positions of the Major Planets*, JPL/Caltech, http://ssd.jpl.nasa.gov/txt/aprx_pos_planets.pdf, last accessed 24/02/2011.
- Tudat working group, *TU Delft Astrodynamics Toolbox*,
<http://tudat.tudelft.nl>, last accessed 10/04/2011, 2011.
- Verhulst, F., *Nonlinear Differential Equations and Dynamical Systems*, 2nd edition, Universitext, 2000.
- Wang, Z., *Computation and Visualization of Invariant Manifolds*, Thesis Report, Concordia University, 2009.
- Wang, Z., *Heteroclinic* <http://www.heteroclinic.net>, last accessed 14/02/2012, 2011.
- Wakker, K.F., *Lecture Notes Astrodynamics I, AE4-874I*, Delft University of Technology, the Netherlands, 2007a.
- Wakker, K.F., *Lecture Notes Astrodynamics II, AE4-874II*, Delft University of Technology, the Netherlands, 2007b.
- Wiggins, S., *Introduction to Applied Nonlinear Dynamical Systems and Chaos*, Springer, 2nd edition, 2003.

Appendix A: Numerical integration

When equations of motion are given in the form of ordinary differential equations, an orbit or manifold can be found by integration. Various methods are commonly used in celestial mechanics, such as the single-step or Runge-Kutta (RK) methods, which are available within Tudat (Appendix B). In this section two versions are presented.

RK integrators

The RK integrators are known to be easy to use and applicable to a variety of problems [Montenbruck, 2005]. They are based on a first-order Taylor expansion:

$$\begin{aligned}y(t_0 + h) &\approx y_0 + h\dot{y}_0 \\ &= y_0 + hf(t_0, y_0) \\ &= y_0 + h\Phi\end{aligned}\tag{74}$$

The increment function Φ can have different forms and order. In Tudat second (Euler), fourth and eighth-order RK integrators are available. For example for the fourth-order Runge-Kutta (RK4) algorithm, referred to as the classical RK, it is defined as:

$$\begin{aligned}k_1 &= f(x(t_0), y(t_0)) \\ k_2 &= f(x(t_0 + h/2), y(t_0) + k_1/2) \\ k_3 &= f(x(t_0 + h/2), y(t_0) + k_2/2) \\ k_4 &= f(x(t_0 + h), y(t_0) + k_3) \\ \Phi &= \frac{k_1}{6} + \frac{k_2}{3} + \frac{k_3}{3} + \frac{k_4}{6}\end{aligned}\tag{75}$$

It is based on derivatives on different places along a function, as shown in figure 49.

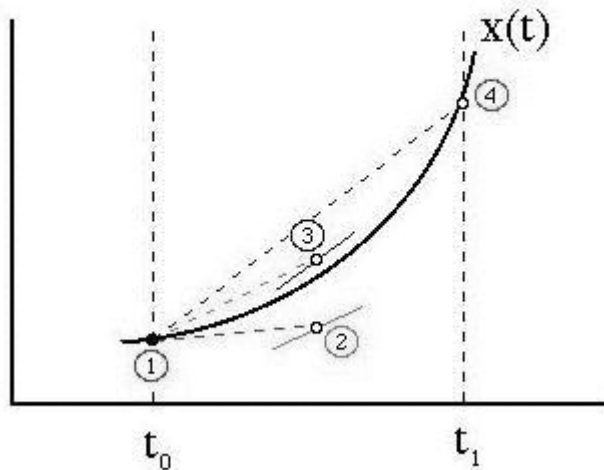


Figure 49: The Runge-Kutta 4th order algorithm [McMillan, 2011].

RK4 approximates the exact solution up to terms of order h^4 . So the truncation error depends on the order of the increment function, in this case:

$$e_{RK4} = |y(t_0 + h) - (y_0 + h\Phi)| \leq \text{constant } h^5 \quad (76)$$

Higher-order RK formulas look like:

$$k_1 = f(t_0 + c_1 h, y_0) k_i = f(t_0 + c_i h, y_0 + h \sum_{j=1}^{i-1} a_{ij} k_j) \quad (77)$$

Such that with given vectors of coefficients b_i the increment function becomes:

$$\Phi = \sum_{i=1}^s b_i k_i \quad (78)$$

The coefficients are in the form of Table 10, which is called the *Butcher tableau*.

$c_0 = 0$				
c_1	a_{10}			
c_2	a_{20}	a_{21}		
$c_s = 1$	a_{s0}	a_{s1}	$a_{s,s-1} = 0$	
	$b_0 = a_{s0}$	$b_1 = a_{s1}$	$b_{s-1} = -\lambda$	$b_s = \lambda$
	$\hat{b}_0 = b_0$	$\hat{b}_1 = b_1$	$\hat{b}_{s-1} = 0$	$\hat{b}_s = 0$
	$\hat{\hat{b}}_0$	$\hat{\hat{b}}_1$	$\hat{\hat{b}}_{s-1}$	$\hat{\hat{b}}_s$

Table 19: Coefficients for higher order RK methods.

Variable step size

For more suitable use of an integrator, the step size can be adjusted according to the required accuracy. This is for example done in the RK-Fehlberg 7(8) integrator (RKF78) [Fehlberg, 1985]. The Fehlberg method requires less computational steps than earlier methods of the same order. It compares the solutions of an approximation of the 7th and of the 8th order to evaluate the accuracy. Both approximations use the same coefficients, hence the reduced computational effort.

The integration method is discussed in detail in [Burden, 2001], which covers the theory that has been implemented in Tudat.

Based on the unit tests that form an important part of Tudat (see Appendix B) both the RK4 and RKF78 integrators are assumed to be accurate enough for the problems in this study. When developing manifolds in Chapter 6 another test is performed to support this. Also the resulting periodic orbits in Chapter 5 show that the integrators as implemented in Tudat are accurate enough.

Appendix B: Tudat

The TUD Astrodynamics Toolbox (Tudat) is a C++ library for astrodynamics simulations developed and maintained by staff and students in the Astrodynamics & Satellite Missions research group at the TUD's faculty of Aerospace Engineering [Tudat working group, 2011].

After various former tools, it was decided to work on a more structured way to share code written for amongst others theses and PhD. studies on Orbital Science and Technology. Tudat is therefore set up with particular focus on modularity and robustness of code.

For development any environment can be used, while the compiler used by Tudat is g++ of the GNU Compiler Collection, which is available for all platforms.

Development

Using Tudat for a thesis also means that active participation in its development is expected. Newly written work packages during the thesis should be incorporated in it and should fulfill certain standards. These concern amongst others development guidelines which are available in a development manual [Tudat working group, 2011] and the Tudat Commandments and Guidelines [Melman, 2011]. The online forum [Tudat working group, 2011] and meetings can be used for support and discussion.

Because of the technical documentation coming with the toolbox, all code should be commented according to Doxygen style [Doxygen, 2011]. This makes it possible to generate documentation straight from the comments.

All code can be found in the repository, such that all changes and the progress of the projects can be tracked. It is checked by the developer by means of unit tests and by other developers. Changes and communication regarding existing code is done via .diff-files. Especially the development of unit tests and the code checking take time and should be taken into consideration when planning programming tasks.

Additions

The last public version is v0.3, but newer versions were downloaded from the repository. Tudat required expansion for specific functionality, such as:

- Approximate planet positions for circular coplanar orbits.
Based on the variation of orbital elements of the J2000 model [Standish, 2011], but only using the semi-major axis as constant radius and the initial and changing mean longitude.
- Equations of motion CR3BP.
Defined by the 6 first-order differential equations used throughout this report and only dependent on mass parameter.
- Calculation mass parameter of a three-body system.
Based on the gravitational parameters as included as planet parameters in Tudat, the mass parameter is calculated after two predefined celestial objects are selected.

- Conversion from normalized to standard parameters.
According to the equations in Chapter 7, time, state and the Jacobian energy constant are converted, given the distance between the two major bodies.
- Determination of libration points.
Based on the equations of Section 2.6 and their derivatives, Newton-Raphson is used to find the x-locations of the collinear libration points. The positions of the equilateral points are computed directly. The positions are only dependent on the mass parameter.
- Generation of periodic orbits by means of differential correction.
Given the initial guess for position and velocity and the mass parameter, differential correction is performed until a fixed number of iterations or a convergence limit. This results in the initial conditions of a planar periodic orbit.
- Computation of the starting points of manifolds.
Starting with the initial conditions of a periodic orbit and its period, one can choose between stable and unstable manifolds and specify the size of the deviation from the periodic orbit and the number of starting points. The function will output this amount of starting points divided equally along the periodic orbit.
- Implementation of stopping condition for integrator.
Previously only integration up to a specific end time was possible within Tudat, so for the fixed step size integrator functionality to integrate up to any stopping condition has been added, as well as adjustment of the step size to accurately find the final state vector.

All new functions come with a unit test and are checked by other developers. Furthermore the outcomes of most functions are verified in detail as described in Chapters 3 to 7.

Appendix C: AUTO

AUTO is a tool to analyze ordinary differential equations and boundary value problems. It can be downloaded online and comes with extensive documentation [Doedel, 2009]. It is used commonly to study the restricted three-body problem [Deurloo, 2003] [Elvik, 2004] [Oldeman, 2011]. During this study version 0.8 of AUTO-07P has been used [AUTO website, 2010], which consists of scripts and demonstrations in Python and runs best using UNIX/Linux-based computers.

Theory

AUTO uses (pseudo-arc length) continuation and bifurcation analysis to come up with solution families for ordinary differential equations [Wang, 2009] [Doedel, 2010]. The solutions families for the libration points in the CR3BP are for example the radial positions, for different mass parameters. The corresponding *bifurcation diagram* is shown in Figure 50.

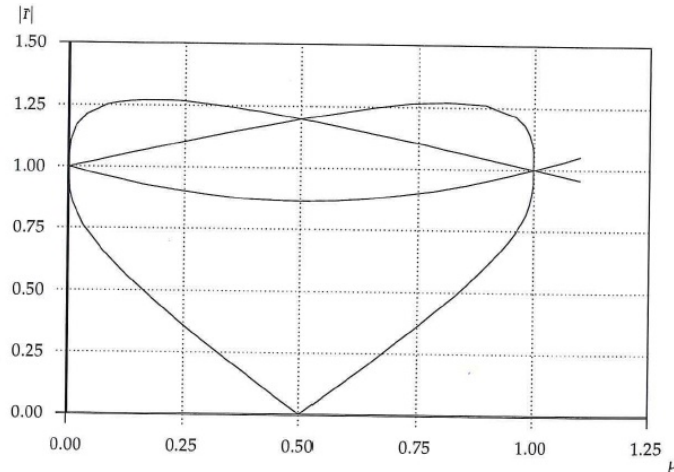


Figure 50: Bifurcation diagram of the position of libration points in the CR3BP [Deurloo, 2003].

First continuation is performed on the 6 first-order differential equations defined by Equation 18 with the mass parameter μ as continuation parameter, to find the libration points. The bifurcation point for $\mu = 0$ (the two-body problem) is found, along with different branches that are continued to the desired value of μ [Deurloo, 2003].

With the selected libration point as the new bifurcation point, the boundary value problem (BVP) for the equations of motion of the CR3BP is given by the same set of differential equations. Time is scaled to the interval $[0,1]$ in the BVP formulation, to find a periodic orbit with period T . Furthermore, for a conservative system with one conserved quantity, an unfolding parameter needs to be added [Calleja, 2011] times the gradient of this conserved quantity, the Jacobian energy constant C :

$$\lambda \left[\frac{\partial C}{\partial x}, \frac{\partial C}{\partial y}, \frac{\partial C}{\partial z}, \frac{\partial C}{\partial v_x}, \frac{\partial C}{\partial v_y}, \frac{\partial C}{\partial v_z} \right] = \lambda [0, 0, 0, v_x, v_y, v_z] \quad (79)$$

The vector field now becomes:

$$\begin{aligned}
\dot{x} &= Tv_x \\
\dot{y} &= Tv_y \\
\dot{z} &= Tv_z \\
\ddot{x} &= T \left(2v_y + x - \frac{(1-\mu)(x+\mu)}{r_1^3} - \frac{\mu(x-1+\mu)}{r_2^3} + \lambda v_x \right) \\
\ddot{y} &= T \left(-2v_x + y - \frac{(1-\mu)y}{r_1^3} - \frac{\mu y}{r_2^3} + \lambda v_y \right) \\
\ddot{z} &= T \left(-\frac{(1-\mu)z}{r_1^3} - \frac{\mu z}{r_2^3} + \lambda v_z \right)
\end{aligned} \tag{80}$$

The boundary conditions for periodicity are [Oldeman, 2011]:

$$\begin{aligned}
x(1) &= x(0) & v_x(1) &= v_x(0) \\
y(1) &= y(0) & v_y(1) &= v_y(0) \\
z(1) &= z(0) & v_z(1) &= v_z(0)
\end{aligned} \tag{81}$$

Here λ is the Floquet multiplier, which determines the stability of the solution and is another unknown during the continuation. The solution branch for $\lambda = 0$ is used to compute the entire family of periodic orbits, other values are used to generate manifolds.

Usage

A demonstration package of scripts and input files called 'r3b' is included in the standard version of AUTO. The files make it amongst others possible to generate families of periodic orbits and manifolds, after libration points have been determined. Only a script to generate periodic orbit and manifolds about L1 is available. It can easily be copied and adjusted, resulting in the L1a.auto and L2a.auto scripts, which are called from r3b.auto.

In general the following steps are taken when using the r3b demo in AUTO:

1. Adjust the value of the mass parameter μ in r3b.auto.
2. Use compute_lps to find the libration points, for the given value of μ .
3. Adjust the index referring to libration points L1 and L2 in compute_lps.
4. Adjust the value for Jacobian energy C_{L_1} or C_{L_2} in c.r3b.L1 to find the corresponding periodic orbit.
5. Use scripts L1a.auto and/or L2a.auto to generate unstable manifolds.
6. Change from Floquet multiplier λ to $\frac{1}{\lambda}$ and use negative step size to generate stable manifolds.

The scripts are adjusted to my needs, such that for example output could be used in other ways. The original data files can be visualized using QTPlaut [Wang, 2011].

The manifolds generated by AUTO have only been used for visual reference, as the theory (as presented in Chapter 6) was easy to implement and a useful addition to Tudat. Other data such as the position of libration points and families of periodic orbits have been used for verification and analysis in Chapters 3 to 7.